Application of Deep Learning to Seismic Event Classification in the Gujarat Region, India

Pragnath Dodda[1], Gudhimella Srijayanthi[2], Johannes Faber[3], Jonas Köhler[3], Wei Li[3], Nishtha Srivastava[3], Santosh Kumar[4], and Sumer Chopra[1]

[1]Institute of Seismological Research
[2]National Geophysical Research Institute
[3]Frankfurt Institute for Advanced Studies
[4]Institute of Seismological Research, Gandhinagar-382009, Gujarat

February 28, 2024

Abstract

In anticipation to substitute the existing manual/semi-automated methods for classifying quarry blasts, earthquakes, and noise, we developed three convolutional neural network (CNN) models. The three CNN models extract relevant features from seismograms (waveform), spectrograms (spectrum), and a combination of the two respectively. A total of 3414 samples were extracted from the three categories, 15% of the data from each category were split for testing, and the remaining data were augmented and used for training. The waveform model, spectrogram model, and combined model achieved accuracies of 95.32%, 93.13%, and 93.96%, respectively. The reliability of these models was ascertained by promising accuracies of >90% and 100% obtained for large and small datasets from testing with SCEDC data and records from the Palitana region (Gujarat) respectively. The results of this study demonstrate the potential of deep learning-based approaches for the effective classification of seismic events.

a

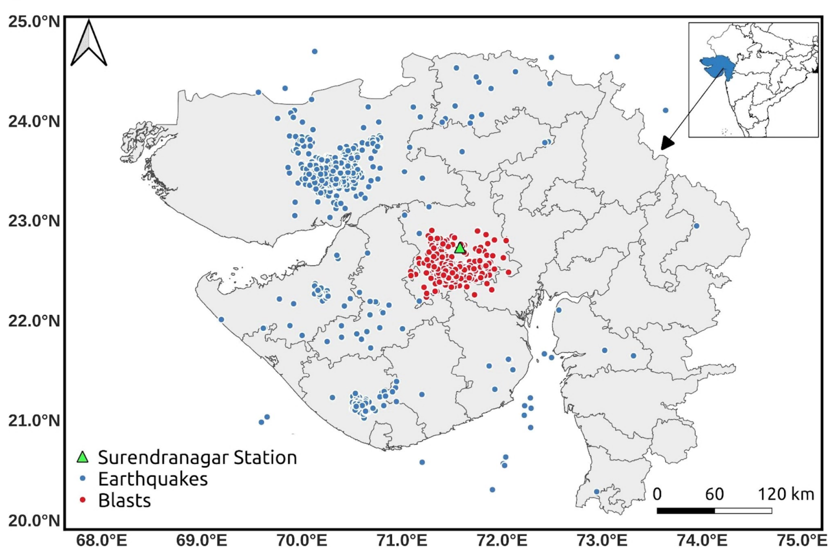

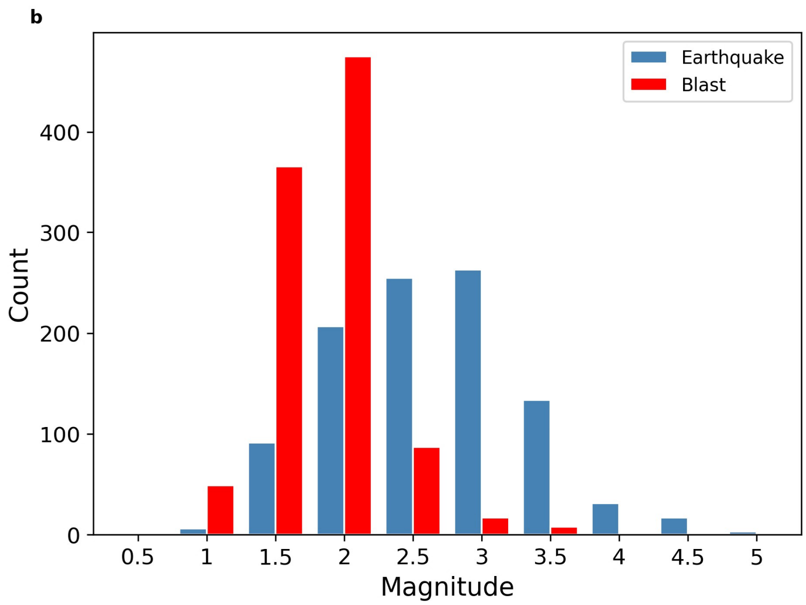
b
Earthquake
Blast
Count
Magnitude
0
100
200
300
400
0.5
1
1.5
2
2.5
3
3.5
4
4.5
5

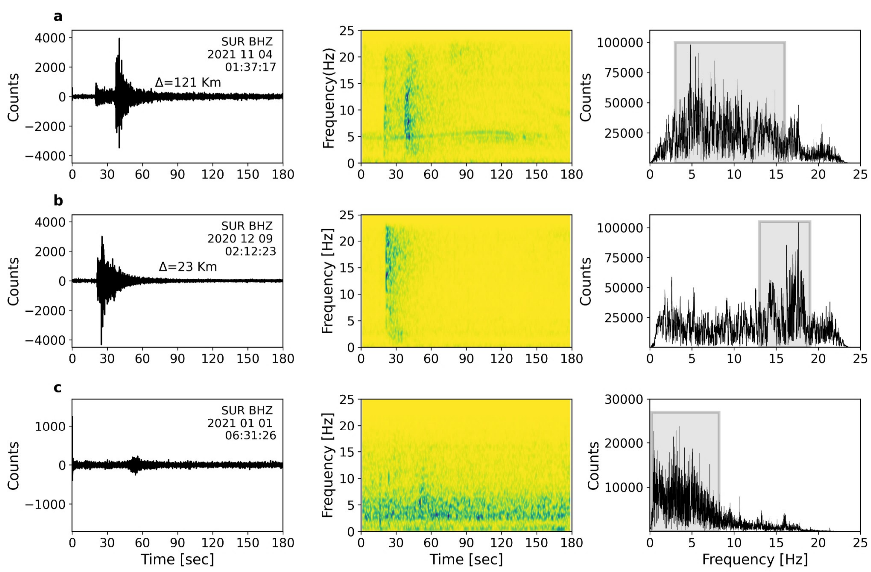
a
SUR BHZ
2021 11 04
01:37:17
Δ=121 Km
b
SUR BHZ
2020 12 09
02:12:23
Δ=23 Km
c
SUR BHZ
2021 01 01
06:31:26
Counts
Frequency(Hz)
Frequency [Hz]
Time [sec]
Frequency [Hz]

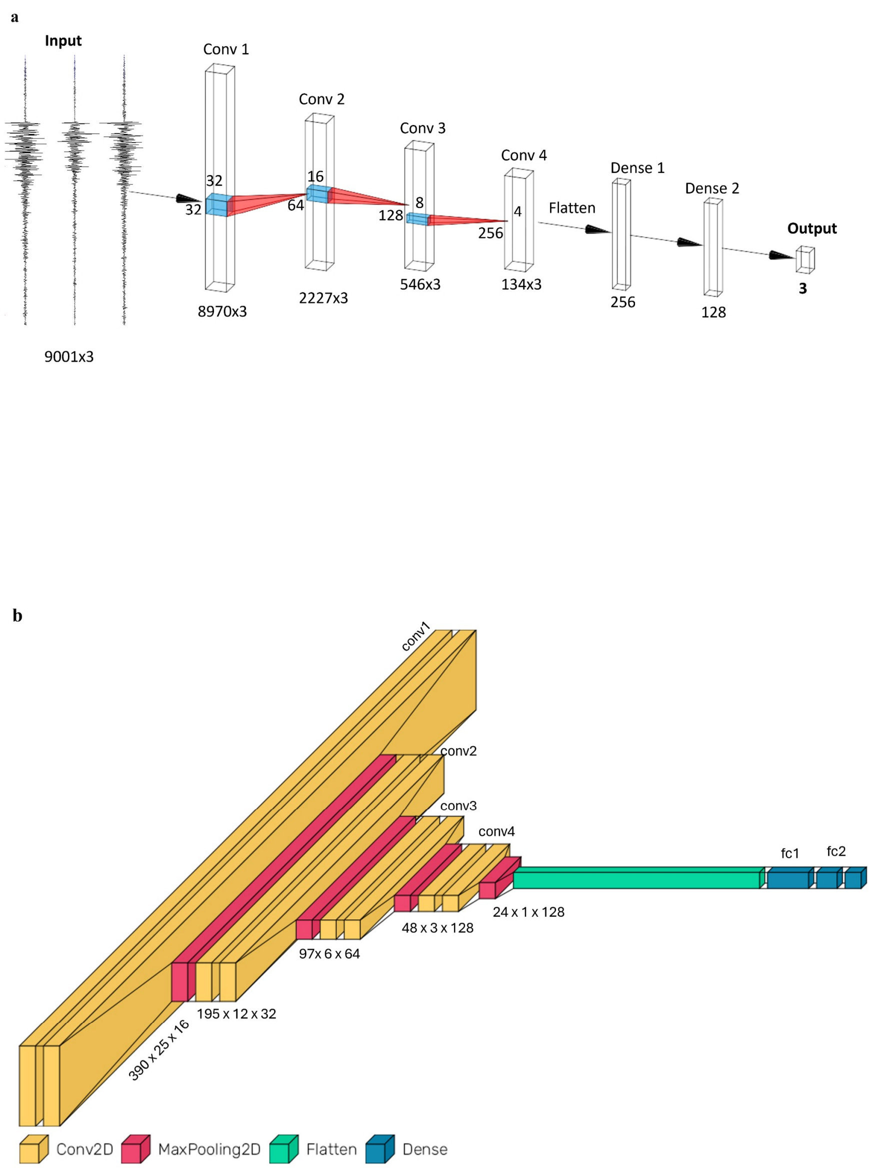

Hosted file

`Table1.docx` available at https://authorea.com/users/745927/articles/717879-application-of-deep-learning-to-seismic-event-classification-in-the-gujarat-region-india

Application of Deep Learning to Seismic Event Classification in the Gujarat Region, India

D. Pragnath [1,3], G. Srijayanthi [1], *, Johannes Faber[2,4], Jonas Köhler[2,4], Wei Li[2], Nishtha Srivatsava [2,4], Santosh Kumar [1], Sumer Chopra [1]

[1] Institute of Seismological Research, Gandhinagar, Gujarat, India

[2] Frankfurt Institute for Advanced Studies, Frankfurt, Germany

[3] Gujarat University, Ahmedabad, Gujarat, India

[4] Goethe Universität, Frankfurt am Main, Germany

*srijayanthi.india@gmail.com

Key Points

- Developed 3 CNN models to classify blasts, earthquakes & noise based on the features extracted from waveform, spectrum & combining both.
- All 3 models have >93% accuracies and exhibit exceeding performance in matrix scores F1, recall and precision.
- These models produce > 90% accuracies when tested on new datasets from SCEDC and Palitana region Gujarat.

Abstract

In anticipation to substitute the existing manual/semi-automated methods for classifying quarry blasts, earthquakes, and noise, we developed three convolutional neural network (CNN) models. The three CNN models extract relevant features from seismograms (waveform), spectrograms (spectrum), and a combination of the two respectively. A total of 3414 samples were extracted from the three categories, 15% of the data from each category were split for testing, and the remaining data were augmented and used for training. The waveform model, spectrogram model, and combined model achieved accuracies of 95.32%, 93.13%, and 93.96%, respectively. The reliability of these models was ascertained by promising accuracies of >90% and 100% obtained for large and small datasets from testing with SCEDC data and records from the Palitana region (Gujarat) respectively. The results of this study demonstrate the potential of deep learning-based approaches for the effective classification of seismic events.

Key Words: Deep Learning, CNN, Earthquakes, Quarry blasts, Noise, Spectrogram, Gujarat.

1. INTRODUCTION

Seismicity monitoring is one of the primary objectives in traditional seismological studies. This process requires manual inspection, which is time-consuming and is often associated with errors and biases. Continuous seismic networks used for monitoring seismicity at local and regional scales are thus contaminated with events other than natural earthquakes (Linville et al., 2019). Therefore, discriminating between a local tectonic event and a mining or quarry blast is a routine yet challenging task for both researchers who compile earthquake catalogs and those monitoring seismic networks (Astiz et al., 2014). Further, identification of blasts and earthquakes becomes especially challenging in near real-time monitoring when both the tectonic earthquakes and anthropogenic sources are in proximity (Whidden & Pankow 2012; Wiemer & Baer 2000; Horasan et al., 2009) and the earthquake location has to be reported in less than 10 minutes of earthquake occurrence.

Traditional seismological methods include manual, semi-automated and automated methods to discriminate between tectonic earthquakes, blasts and noise. Initially, the identification was based on occurrence time and location, often represented by the day-night distribution plot. Explosions usually occur during working hours from the same location, unlike earthquakes that can happen at any time and from any location. Later, more technical discrimination techniques were adopted based on waveform and spectrum analysis, such as ratios of amplitudes of various seismic phases (Bennett & Murphy 1986; Wüster et al., 1993; Anderson et al., 2009; Mc Laughlin et al., 2004), velocity spectra assessment (Taylor et al., 1988; Kim et al., 1994; Gitterman et al., 1998; Walter et al., 1995), ratios of corner frequencies (Korrat et al., 2022) and power spectral densities (Sertcelik et al., 2020). For large magnitude earthquakes (M>4), even the moment tensor solutions can be used for identifying the source. However, all these methods may not be applicable in all scenarios and are restricted by magnitude, distance and the type of instrument used to record these seismic signals. Moreover, manual methods are time consuming, require substantial effort for data selection, extraction, conversion and computation of the parameters and subsequent labeling of seismic events as blasts, earthquakes and noise. Unlike certain selection criteria such as window length for estimating amplitude, spectra, or magnitude, choosing corner frequencies and appropriate methods require individual experience and knowledge to ensure the correctness of the obtained results, which can vary for different scenarios. This can lead to partial loss of information or subjective factors affecting the outcome.

Machine learning based classification models can overcome these challenges by preserving all parameter information based on the original waveform data and avoiding the impact of subjective experience on classification outcomes. The advent of machine learning (ML) techniques has significantly impacted various scientific disciplines, including seismology, leading to numerous publications on ML and deep learning-based models for seismic signal classification (Renouard et al., 2021; Linville et al., 2019; Saad et al., 2019, 2022; Li et al., 2022). In the present study, three CNN architectures were developed to identify earthquakes, quarry blasts and seismic noise. The first architecture is based on waveform analysis, the second on spectrum analysis, and the third on a combination of both waveform and spectrum features. The accuracies of all the three models were $\geq$ 93%.

2. DATA

2.1 Data collection

The Gujarat State Seismic Network (GSNet), operated by the Institute of Seismological Research (ISR), Gandhinagar, has been well-maintained since July 2006 (Chopra et al., 2008). The network consists of 60 Broadband Seismograph Stations (BBS) spread throughout the state and neighboring areas. Data from 45 BBS were transmitted to the Institute of Seismological Research via VSAT, enabling near real-time (24 $\times$ 7) monitoring of earthquake activity. Over the years, the network has recorded a significant number of earthquakes, primarily from Kachchh, Saurashtra, and mainland regions of Gujarat state (Rastogi et al., 2013). ISR is also obligated to promptly provide a preliminary earthquake report of all the earthquakes with magnitudes $M \geq 2.5$. These reports should be transmitted within minutes of the earthquake occurrence to both the disaster management authorities and state emergency response center through various modes of communication like email, SMS and the web. A recent study by Kumar et al., (2021) indicated an increase in low-magnitude earthquakes in the past decade, clustering mainly near Surendranagar region in the Saurashtra peninsula and Godhra in the mainland regions, predominantly during daytime (IST). These events were associated with high b-values and were initially suspected to be quarry blasts; this anticipation was later confirmed during the Corona lockdown period. Consequently, the identification of such quarry blasts in the seismic catalog is crucial to provide an earthquake catalog devoid of artificial/anthropogenic events.

In the present study, to differentiate earthquakes, quarry blasts and seismic noise, we utilized the waveform data recorded at Surendranagar (SUR) station from 2007 to 2022. The SUR station (71.580 N, 22.730 E) was chosen as it is a permanently established long-running station of GSNet and also has clear records of anthropogenic activities. The station was equipped with a CMG-3T seismometer, configured at 50 Hz. We identified a total of 1298 blasts, which were ~25 to 37 km from the SUR station, within a region associated with mining-related quarries (Kumar et al., 2021) (Figure 1a). The magnitude range of these blasts (~M 0.6 to M 3.5) closely matches the range of micro earthquakes. Additionally, we selected 1005 local earthquake waveforms with epicentral distances ranging from 30 km to 110 km across Gujarat in the magnitude range of M 0.7 to M 4.5. The earthquakes were carefully chosen with a considerable overlap in the lower magnitude range to have comparable waveforms in the lower magnitude range as in the blast's dataset. To create a uniform dataset of seismic noise, we randomly selected 1111 noise samples encompassing different times of the day and seasons throughout the year. This approach ensures that the dataset represents all possible noise scenarios over different times, seasons and years. The magnitude distribution of the blasts and earthquakes used in the present study were shown in Figure 1b.

Seismological waveform data are a conglomeration of multiple factors like nature of the source, epicentral distance, the travel path/medium and the station location or the underlying geology that mostly influences the noise characteristics. The quality of waveforms (clear seismic phases) also hugely depends on the magnitude as well. It is a challenging job to identify clear phases in the case of lower magnitudes where the energy quickly attenuates resulting in low signal to noise ratio and weak phases that can hardly surpass the background noise level (Korrat et al., 2022; Tibi et al., 2019). Considering all the above-mentioned factors, we employed a 180 s window length for earthquakes, blasts, and noise unlike other published models (Liu et al., 2021; Kong et al., 2022) that utilized ≤ 100s window length. The longer waveform length was chosen to preserve features such as coda length, which differs significantly between earthquakes and blasts, especially for earthquakes with large magnitudes and epicentral distances, resulting in longer coda lengths.

Each earthquake and blast were manually verified and visually inspected based on occurrence time (7 am to 7 pm IST), geographical location, and waveform characteristics, including coda length and P, S phase amplitudes. Furthermore, we observed that identifying the source characteristics is much simpler in the frequency domain than in the time domain (Korrat et al., 2022), as the spectrogram illustrates the signal intensity across different frequencies found within an arbitrary waveform. We plotted spectrograms that provided a clear identification of the source, particularly when categorizing events in the lower magnitude range with low signal-to-noise ratios (Allmann et al., 2008). The spectrum of earthquakes exhibited two distinct frequency bands corresponding to P and S phases in the chosen window length (Figure 2a). Conversely, the spectrum of blasts showed a single band corresponding to the onset of the P phase (Figure 2b). An example of the seismic noise spectrum is shown in Figure 2c. Therefore, a total of 3414 waveforms that include 1298 blasts, 1005 earthquakes and 1111 noise samples were labeled for further processing.

2.2 Data pre-processing and splitting

The most commonly observed issue in seismic waveforms is that traces deviate from the baseline and are associated with some long periodic trend (Liu et al., 2021). Therefore, all the waveforms are corrected for the trend and mean using detrend and demean tools in ObsPy (Breckpot et al., 2010; Krischer et al., 2015). As the first step in deep learning a test dataset, comprising 15% of the raw/unaugmented data, was separated. This test dataset was not used to train the model, and its purpose was to assess the statistical significance of the model's performance. The test set consists of 513 seismic events, almost equally weighted among the three classes; earthquakes (151), blasts (195) and noise (167). The same test dataset was used for all the three models, namely the waveform, spectrum and combined model.

2.3 Data Augmentation

The crux of deep learning models largely depends on the quality, quantity, and consistency of the labeled dataset used for training. Therefore, a limitation of machine learning is the lack of sufficient amount of training data or uneven class balance in a dataset. The present objective for the 3-class classification requires a huge dataset, but the dataset consists of 2901 waveforms which is insufficient for deep learning. So, we adopted the technique of data augmentation to overcome this limitation and construct a suitable training dataset using ObsPy. The data is augmented by: (i) flipping the polarities of the waveforms, (ii) applying bandpass filter from 2.0 Hz to 8.0 Hz and, (iii) randomly muting one trace. The miniseed files are converted into Numpy (Harris et al., 2020) arrays and are saved in '.npy' format with a shape of (9001, 3), where 9001 represents the 'npts' (number of points) and 3 represents the number of channels. In order to maintain uniform trace length or equal number of 'npts', the traces with shorter lengths were padded with zeros at the end. This resulted in a total of 11,614 waveforms that were used as training dataset for the waveform model.

The spectra are computed for the raw waveforms after correcting for the trend and mean. The data augmentation in waveforms shows noticeable changes especially when the polarities of the waveform were flipped. However, such differences/changes were not visually identifiable in the spectrograms. Therefore, the spectrum data of the earthquakes, blasts and noise were augmented by applying band-pass (2.0-8.0 Hz), low-pass (8.0 Hz), and high-pass (2.0 Hz) filters. The input shape for the spectrum model was (390, 25, 3), corresponding to (time × frequency × channels). To maintain the same shape, zero padding was applied at the end of the spectrum data.

3 CNN MODELS

Recent studies have highlighted the effectiveness of CNN-based identification methods in seismic data processing and the extraction of characteristic features. These features can aid in discrimination and classification based on pixel-level information, thereby synthesizing global information. In the present study, we developed three CNN models based on waveforms, spectrograms and combined parameters to classify local earthquakes, quarry blasts and seismic noise. To build these models, TensorFlow (Abadi, 2016) was utilized and all the three models were trained on the Nvidia RTX A5000. Each of these models were described below. All the models were trained on the data recorded at a single station SUR.

A Categorical Cross-Entropy loss function and an Adam optimization method (Kingma et al., 2014) were used to train all the models below. To prevent our models from overfitting data, we incorporated an early stopping mechanism. This means that if the accuracy remains unchanged for selected consecutive epochs (which can be defined through the parameter called “patience"), the training process terminates. This approach ensures the reliability of the training process. In the present study, we chose patience as 10 for all the three models.

3.1 Waveform Model

For training the waveform CNN model, three-component seismogram data with a length of 180s (20s before and 160s after the first arrival) was utilized. For distinguishing the three classes (earthquakes, quarry blasts and noise) we developed a 4 layered convolutional model with filter counts 32, 64, 128 and 256. The model has two fully connected (FC) layers (256, 128) with max-pooling and drop-out layers between each layer show in Figure 3(a). The probability of each class was computed from the output layer using the 'softmax' activation function (Nwankpa et al., 2018). The best accuracy of 95.32 % was obtained with a learning rate of $2*10^{-4}$ and a batch size of 16 given in Table S1 in of Supporting Information.

3.2 Spectrum Model

This model was developed as an alternative approach to discriminate earthquakes and quarry blasts based on spectrograms. Extracting information from spectrograms provides a reliable classification. The spectrograms show clear distinguishing features that can be used to train the model for reliable classification, even in the low-to-intermediate magnitude range of earthquakes and quarry blasts. The spectrograms are computed for 1s sliding windows with 50% overlap, which results in 390-time windows for which we compute the discrete Fourier transform between 1 and 25 Hz for the three components of the seismogram each having 180 s data length. Thus, the spectrogram's model input size is (390 × 25 × 3). Spectrum model focuses on different frequency bands generated due to the arrival of different phases (P and S) to make the three-class identification. This model consists of 4 convolution layers with 16, 32, 64 and 128 filters, and two fully connected layers at the end. We applied a 2 × 2 'max-pooling' between each convolution layer and the final layer is the fully connected output layer that computes the probabilities obtained for different classes using the 'softmax' activation function shown in Figure 3(b). The activation function used for this model is SeLU and an accuracy of 93.13% is obtained.

3.3 Combined Model

The combined model was developed combining the architectures of waveform and spectrogram models incorporating the features from both waveform and spectrum. The features thus extracted from both the models are then combined with a concatenation layer. The concatenated features are then passed through a FC layer before the model predicts the final classification shown in Figure S1. The SeLU activation function was used across the network appended by a last layer of softmax activation function with three neutrons for a 3-category classification problem. An accuracy of 93.96 % was obtained using this model.

4. RESULTS AND DISCUSSION

In this study, we employed a training dataset comprising 11,614 waveforms and a test dataset of 513 waveforms to build three models namely waveform, spectrogram and combined. The achieved accuracies for these models were 95.32%, 93.13%, and 93.96%, respectively. Further, the performance of these models were assessed using Receiver Operating Characteristic (ROC) curves on the test dataset. These curves are useful for testing the model's ability to classify input by plotting the true positive rate against the false positive rate. The Area Under the Curve (AUC) was employed as a metric to measure the quality of the ROC curve, with a value of 1 signifying optimal performance (Figure S2), the AUC values of each model with individual class values are given in Table S2. The AUCs are >0.97 for each model indicating the model's ability to correctly distinguish various classes (Table S2)

In ML, to evaluate the performance of a classification of models these four parameters are used namely, accuracy (Acc), precision (Pr), recall (Re) and F1-score (F1).

$$\text{Acc} = \frac{TP + TN}{FP + TP + TN + FN} \quad (1)$$

$$\text{Pr} = \frac{TP}{TP + FP} \quad (2)$$

$$\text{Re} = \frac{TP}{TP + FN} \quad (3)$$

$$\text{F1} = 2\ \frac{Re * Pr}{Re + Pr} \quad (4)$$

where, TP and TN are abbreviations for True Positive and True Negative, similar to FP and FN, which represent False Positive and False Negative. Accuracy (1) describes the correctness rate of the predicted labels, as it is the ratio of the sum of all the true predictions to the number of all possible predictions. The precision (2) value provides insights into TP (such as earthquake, blast, or noise in our case), where a value close to 1 indicates that most predictions are correctly identified. Recall (3) is the ratio of positively identified predictions to the number of actual positive classes. Thus, a higher recall value suggests that most predictions are correct, reducing the possibility of misclassification or false classification. The F1-score (4), unlike its counterparts recall and precision, considers both true and false predictions and is a weighted average of precision and recall. These parameters are calculated for each model and tabulated in table T1. These four parameters are >0.90 in all the three models. The precision value obtained from the waveform model is highest (0.97) for noise and earthquakes, indicating that these classes are better or correctly identified compared to the blasts that have least precision value (0.91). However, in the spectrum model, the ability to predict the blasts improves, indicating an increase in precision value (0.96) compared to the waveform model. Further, the confusion matrix provides detailed insights on the actual number of true and predicted classes in each category. The confusion matrix of the three models (Figure S3) shows the edge of each model over the other. Although the waveform model gives best predictions in all the categories, the combined model gives 100% correct prediction in the noise class. The same was expected from the spectrum model that was developed based on the difference observed in the predominant frequencies of blasts, noise and earthquakes (Figure 2). However, it failed to produce the expected outcome.

The waveform model produces the highest accuracy when compared to other models developed in the present study, and its performance is also comparable with the previously published waveform-based CNN model (Liu et al., 2021) to distinguish tectonic and non-tectonic earthquakes. Their model was trained and tested using data from the China Earthquake Network Center. They obtained an accuracy of 92% with their four layered model using the Rectified Linear Unit (ReLU) activation function in a 7-layered CNN model. In another study, Hourcade et al. (2022) developed a 4-layered spectrum-based CNN model with the ReLU activation function. There model was trained to differentiate between natural and anthropogenic events from metropolitan France, and it achieved an accuracy of 98%.

4.1 Misclassifications by Waveform-based CNN

The waveform-based model identifies noise with high accuracy (99%). However, a small proportion of the test set (4%, comprising 22 waveforms) was misclassified, primarily consisting of blasts and earthquakes. A visual examination of the misclassified waveforms was conducted (Figure S4) to identify any specific patterns or features that are contributing to the misclassification of certain waveforms. Subsequently, the signal-to-noise ratio (SNR) was also calculated using the following formula to quantify the limitations of the waveform-based model with respect to the relative strength of the seismic signal to the background noise.

$$SNR = 10\, log_{10}\left(\frac{\mu\, S^2}{\mu\, N^2}\right) \qquad (5)$$

where, $\mu\, S^2$ represents the mean squared amplitude of the seismic signal calculated over a 10 s interval post the first arrival, and $\mu\, N^2$ represents the mean squared amplitude of background noise calculated over a 10 s interval preceding the first arrival (Figure S5).

The resulting SNR value, expressed in decibels (dB), provides a measure of the relative strength of the seismic signal to the background noise. In the present study the SNR varies from -9 to 44 dB (Figure S6). The negative values are obtained when the ratio of $\left(\frac{\mu\, S^2}{\mu\, N^2}\right)$ is < 1 which indicates that the noise dominates over the signal. $\left(\frac{\mu\, S^2}{\mu\, N^2}\right)$=1 means that the strength of signal and noise are equal, resulting in a SNR of 0 (as $10\ log_{10}$ (1) = 0). Majority of the misclassified waveforms (15 i.e. 68% of the total misclassified waveforms) have low SNR <10 (Figure S6 (c)) and ≥ 50% prediction probability for the wrong class given in Figure S7.

4.2 Misclassification by Spectrogram-based CNN

A clear distinction between an earthquake and a quarry blast was evident on a spectrogram (Figure 2), prompting us to develop a spectrum-based model to improve the accuracy of classification. Although the spectrum model achieved good classification results, they were not as promising as anticipated. Visual inspection of the misclassified spectrogram records revealed two issues: (1) strong and consistent energy at a particular frequency band throughout the selected time window, and (2) a frequency response resembling a sinusoidal trend from an unidentified source (example shown in Figure S8). Attempts to mitigate these issues by applying a bandstop filter resulted in the loss of information and created a void at that particular frequency band (Figure S8(b)). An improved dataset would provide a more comprehensive understanding of the model's behavior and enhance its robustness, which is currently limited by the limited dataset.

5. INDEPENDENT TEST

The three models developed in the present study were mainly trained using GSNet data. However, to make sure they work well in different situations, we tested them using earthquake data from the Southern California Earthquake Data Center (SCEDC). A total of 1037 events were downloaded, with 417 earthquakes recorded at BJX station and 620 blasts recorded at EDW2 station. An accuracy of 94%, 90% and 91% was obtained with waveform model, spectrum and combined model respectively results were given in Fig S9.

Further, while preparing this manuscript, we observed some unexpected seismic activity from a region named Palitana, in the Gujarat state of India, hitherto devoid of any active seismic activity from previous GSNet monitoring for almost 16 years. Thus, we tested these few ambiguous waveforms, and with 100% certainty, these events were classified correctly as quarry blasts with all our three models.

6. CONCLUSION

In order to reduce the amount of processing time for classifying various seismic events, in the present study we developed three deep learning classification models based on waveform, spectrogram, and combining both utilizing the CNNs. These models identified seismic noise, quarry blasts, and earthquakes with an accuracy of 95.32%, 93.13%, and 93.96% respectively. To verify the dependability and efficacy of these models, tests were conducted on alternative datasets. This testing provided us clear evidence that these models can be effectively utilized for classification of seismic events (earthquakes & blasts) from other regions as well. The accuracy and application of our models to different regions can be further effectively improved by increasing our labelled dataset with varied examples.

The ML based approaches are more efficient and accurate in discriminating earthquakes and blasts over manual methods that are limited by magnitude and SNR. In the present study, 185 waveforms have SNR < 10, which means that the noise is dominant over the signal and only 15 (8% of 185 waveforms) were misclassified and 92% of the events were correctly classified, even in the low magnitude range and noisy data. The proposed classification models can improve the speed and accuracy in detecting the microseismic events and quarry blasts. This approach can be used to discriminate in real time and reduce the mislabelled/ambiguous events and thus constituting in making the catalog as reliable as possible. On a long-term basis we plan to use these models for monitoring illegal mining activity in Gujarat state as such activities demand attention from local governing bodies which may cause important implications for the safety and environmental management.

7. FUTURE WORK

These classification models will be further developed for near real time monitoring which includes phase detection and estimating the earthquake location parameters. This should be able to reduce the manual efforts to identify different sources and also estimate the location and magnitude within a fraction of seconds. Recent works utilized Fourier Neural Operators (Li et al., 2020; Sun et al., 2023) to develop near real time seismic monitoring. They proposed a model to identify the earthquakes and mark phases on the real time monitoring with multiple stations as input.

ACKNOWLEDGEMENTS

We acknowledge the support of the Department of Science and Technology, Government of Gujarat in establishing the broadband seismological network (GSNet) in Gujarat region. We would like to extend our sincere gratitude to FIAS for generously sharing their expertise in AI/ML. Their week-long course on AI/ML played a pivotal role in framing and guiding our work on this problem. Johannes Faber, Jonas Köhler, Wei Li and Nishtha Srivastava acknowledge the support by the Bundesministerium für Bildung und Forschung – BMBF for the "KI-Nachwuchswissenschaftlerinnen" – grant SAI 01IS20059

DATA AVAILABILITY

The data used in the study from Gujarat region (India), will be available on request to the Director General of the Institute of Seismological Research, Gandhinagar, Gujarat, India. The data used for testing (mentioned in section 5) can be downloaded from "https://scedc.caltech.edu/data/waveform.html".

References

Abadi, M. 2016. TensorFlow: learning functions at scale. In Proceedings of the 21st ACM SIGPLAN international conference on functional programming, 1-1.

Allmann, B. P., Shearer, P. M., & Hauksson, E. (2008). Spectral discrimination between quarry blasts and earthquakes in southern California. Bulletin of the Seismological Society of America, 98(4), 2073-2079.

Anderson, D. N., Walter, W. R., Fagan, D. K., Mercier, T. M., & Taylor, S. R. (2009). Regional multistation discriminants: Magnitude, distance, and amplitude corrections, and sources of error. Bulletin of the Seismological Society of America, 99(2A), 794-808.

Astiz, L., Eakins, J. A., Martynov, V. G., Cox, T. A., Tytell, J., Reyes, J. C., ... & Vernon, F. L. (2014). The Array Network Facility seismic bulletin: Products and an unbiased view of United States seismicity. Seismological Research Letters, 85(3), 576-593.

Bennett, T. J., & Murphy, J. R. (1986). Analysis of seismic discrimination capabilities using regional data from western United States events. Bulletin of the Seismological Society of America, 76(4), 1069-1086.

Breckpot, R., & Marzec, M. K. (2010). ObsPy: a python toolbox for seismology, a data center perspective. Seismol. Res. Lett., 81(3), 530-533.

Chopra, S., Yadav, R. B. S., Patel, H., Kumar, S., Rao, K. M., Rastogi, B. K., ... & Srivastava, S. (2008). the gujarat (india) seismic network. Seismological Research Letters, 79(6), 806-815.

Gitterman, Y., Pinsky, V., & Shapira, A. (1998). Spectral classification methods in monitoring small local events by the Israel seismic network. Journal of seismology, 2, 237-256.

Harris, C. R., Millman, K. J., Van Der Walt, S. J., Gommers, R., Virtanen, P., Cournapeau, D., ... & Oliphant, T. E. (2020). Array programming with NumPy. Nature, 585(7825), 357-362.

Horasan, G., Güney, A. B., Küsmezer, A., Bekler, F., Öğütçü, Z., & Musaoğlu, N. (2009). Contamination of seismicity catalogs by quarry blasts: an example from Istanbul and its vicinity, northwestern Turkey. Journal of Asian Earth Sciences, 34(1), 90-99.

Hourcade, C., Bonnin, M., & Beucler, É. (2023). New CNN-based tool to discriminate anthropogenic from natural low magnitude seismic events. Geophysical Journal International, 232(3), 2119-2132.

Kim, W. Y., Simpson, D. W., & Richards, P. G. (1994). High-frequency spectra of regional phases from earthquakes and chemical explosions. Bulletin of the Seismological Society of America, 84(5), 1365-1386.

Kingma, D. P., & Ba, J. (2014). Adam: A method for stochastic optimization. arXiv preprint arXiv:1412.6980.

Kong, Q., Wang, R., Walter, W. R., Pyle, M., Koper, K., & Schmandt, B. (2022). Combining Deep Learning With Physics Based Features in Explosion-Earthquake Discrimination. Geophysical Research Letters, 49(13), e2022GL098645.

Korrat, I. M., Lethy, A., ElGabry, M. N., Hussein, H. M., & Othman, A. S. (2022). Discrimination between small earthquakes and quarry blasts in Egypt using spectral source characteristics. Pure and Applied Geophysics, 179(2), 599-618.

Krischer, L., Megies, T., Barsch, R., Beyreuther, M., Lecocq, T., Caudron, C., & Wassermann, J. (2015). ObsPy: A bridge for seismology into the scientific Python ecosystem. Computational Science & Discovery, 8(1), 014003.

Kumar, S., Kumar, R. C., Roy, K. S., & Chopra, S. (2021). Seismic monitoring in Gujarat, India, during 2020 coronavirus lockdown and lessons learned. Seismological Research Letters, 92(2A), 849-858.

Li, W., Chakraborty, M., Sha, Y., Zhou, K., Faber, J., Rümpker, G., ... & Srivastava, N. (2022). A study on small magnitude seismic phase identification using 1D deep residual neural network. Artificial Intelligence in Geosciences, 3, 115-122.

Li, Z., Kovachki, N., Azizzadenesheli, K., Liu, B., Bhattacharya, K., Stuart, A., & Anandkumar, A. (2020). Fourier neural operator for parametric partial differential equations. arXiv preprint arXiv:2010.08895.

Linville, L., Pankow, K., & Draelos, T. (2019). Deep learning models augment analyst decisions for event discrimination. Geophysical Research Letters, 46(7), 3643-3651.

Liu, X., Ren, T., Chen, H., & Chen, Y. (2021). Classification of tectonic and non-tectonic seismicity based on convolutional neural network. Geophysical Journal International, 224(1), 191-198.

McLaughlin, K. L., Bonner, J. L., & Barker, T. (2004). Seismic source mechanisms for quarry blasts: modelling observed Rayleigh and Love wave radiation patterns from a Texas quarry. Geophysical Journal International, 156(1), 79-93.

Nwankpa, C., Ijomah, W., Gachagan, A., & Marshall, S. (2018). Activation functions: Comparison of trends in practice and research for deep learning. arXiv preprint arXiv:1811.03378.

Rastogi, B. K., S. Kumar, and S. Aggarwal (2013). Seismicity of Gujarat, Nat. Hazards 65, no. 2, 1027–1044.

Renouard, A., Maggi, A., Grunberg, M., Doubre, C., & Hibert, C. (2021). Toward false event detection and quarry blast versus earthquake discrimination in an operational setting using semiautomated machine learning. Seismological Society of America, 92(6), 3725-3742.

Saad, O. M., Shalaby, A., & Sayed, M. S. (2019). Automatic discrimination of earthquakes and quarry blasts using wavelet filter bank and support vector machine. Journal of Seismology, 23, 357-371.

Saad, O. M., Soliman, M. S., Chen, Y., Amin, A. A., & Abdelhafiez, H. E. (2022). Discriminating earthquakes from quarry blasts using capsule neural network. IEEE Geoscience and Remote Sensing Letters, 19, 1-5.

SCEDC (2013): Southern California Earthquake Data Center. Caltech. Dataset. doi:10.7909/C3WD3xH1.

Sertçelik, F., Yavuz, E., Birdem, M., & Merter, G. (2020). Discrimination of the natural and artificial quakes in the Eastern Marmara Region, Turkey. Acta Geodaetica et Geophysica, 55, 645-665.

Sun, H., Ross, Z. E., Zhu, W., & Azizzadenesheli, K. (2023). Next-Generation Seismic Monitoring with Neural Operators. arXiv preprint arXiv:2305.03269.

Taylor, S. R., Sherman, N. W., & Denny, M. D. (1988). Spectral discrimination between NTS explosions and western United States earthquakes at regional distances. Bulletin of the Seismological Society of America, 78(4), 1563-1579.

Tibi, R., Linville, L., Young, C., & Brogan, R. (2019). Classification of local seismic events in the Utah region: A comparison of amplitude ratio methods with a spectrogram-based machine learning approach. Bulletin of the Seismological Society of America, 109(6), 2532-2544.

Walter, W. R., Mayeda, K. M., & Patton, H. J. (1995). Phase and spectral ratio discrimination between NTS earthquakes and explosions. Part I: Empirical observations. Bulletin of the Seismological Society of America, 85(4), 1050-1067.

Whidden, K. M., & Pankow, K. L. (2012). A catalog of regional moment tensors in Utah from 1998 to 2011. Seismological Research Letters, 83(5), 775-783.

Wiemer, S., & Baer, M. (2000). Mapping and removing quarry blast events from seismicity catalogs. Bulletin of the Seismological Society of America, 90(2), 525-530.

Wüster, J. (1993). Discrimination of chemical explosions and earthquakes in central Europe—a case study. Bulletin of the Seismological Society of America, 83(4), 1184-1212.

Tables and captions

Table 1: Summary of the evaluation parameters obtained for waveform (WF), spectrum (SPEC) and combined (COM) models.

Classes	**F1 Score**			**Recall**			**Precision**		
	WF	SPEC	COM	WF	SPEC	COM	WF	SPEC	COM
Earthquake	0.91	0.95	0.95	0.92	0.97	0.94	0.97	0.94	0.96
Blasts	0.93	0.92	0.93	0.95	0.89	0.92	0.91	0.96	0.93
Noise	0.98	0.97	0.98	0.99	0.98	0.99	0.97	0.96	0.96

436 **Figures and Figure Captions**

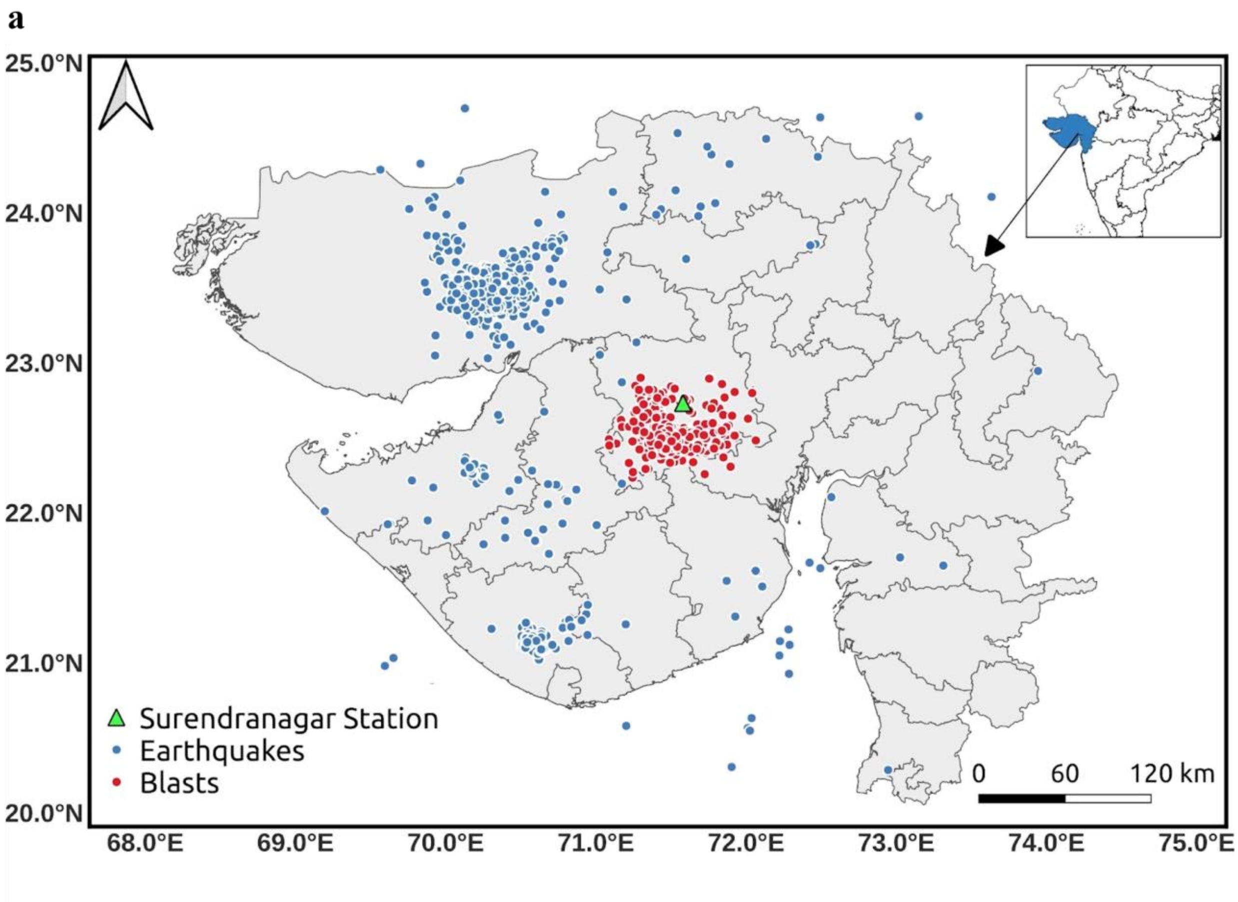

437

438 Figure 1(a): The spatial distribution of the earthquakes (blue circles) and blasts (red circles) used
439 in the present study, recorded at Surendranagar (SUR) broadband station (green triangle). The inset
440 map shows the Gujarat State in India.

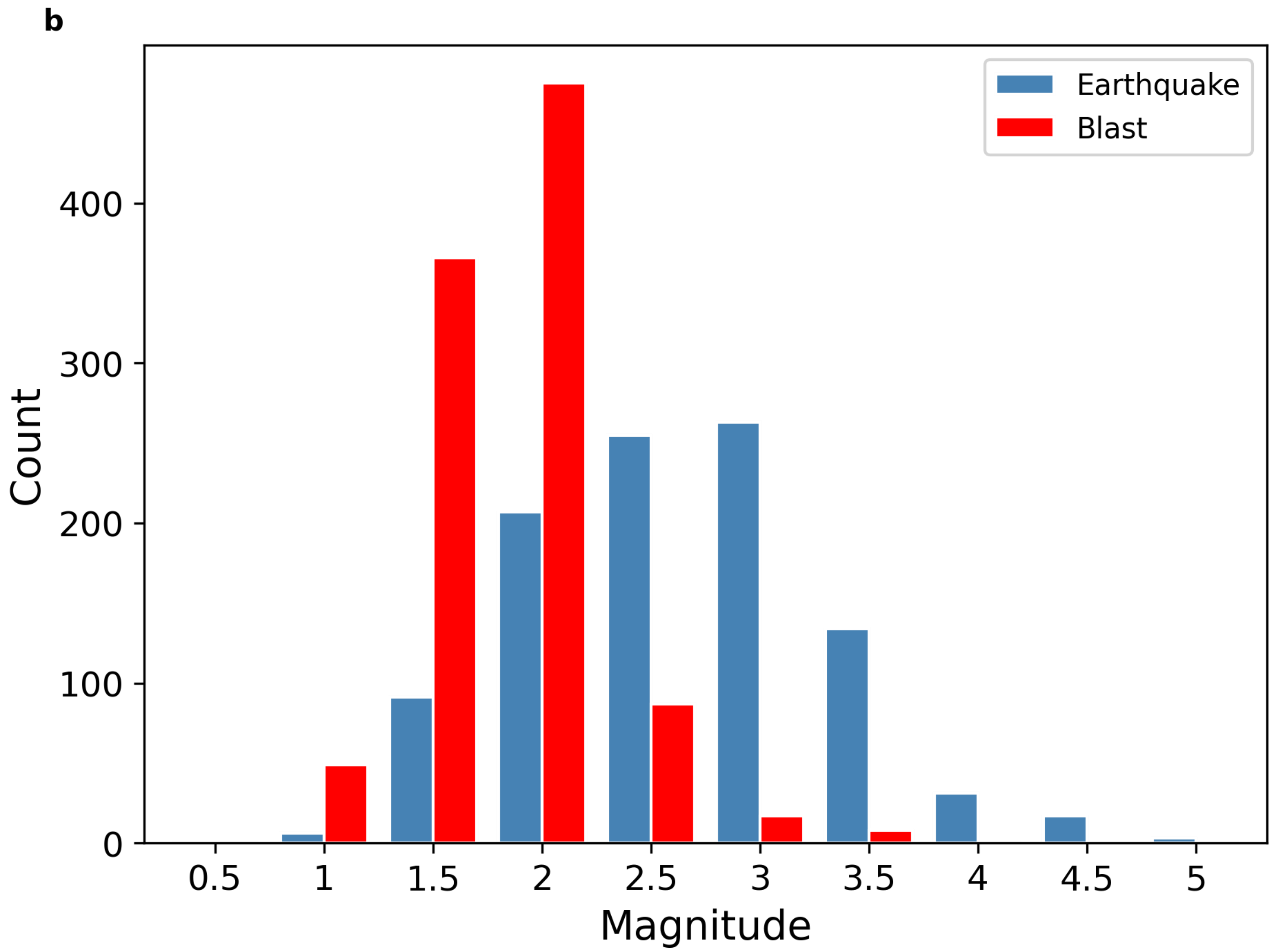

Figure 1(b): Magnitude distribution of the blasts and earthquakes (shown in figure 1) used in the present study.

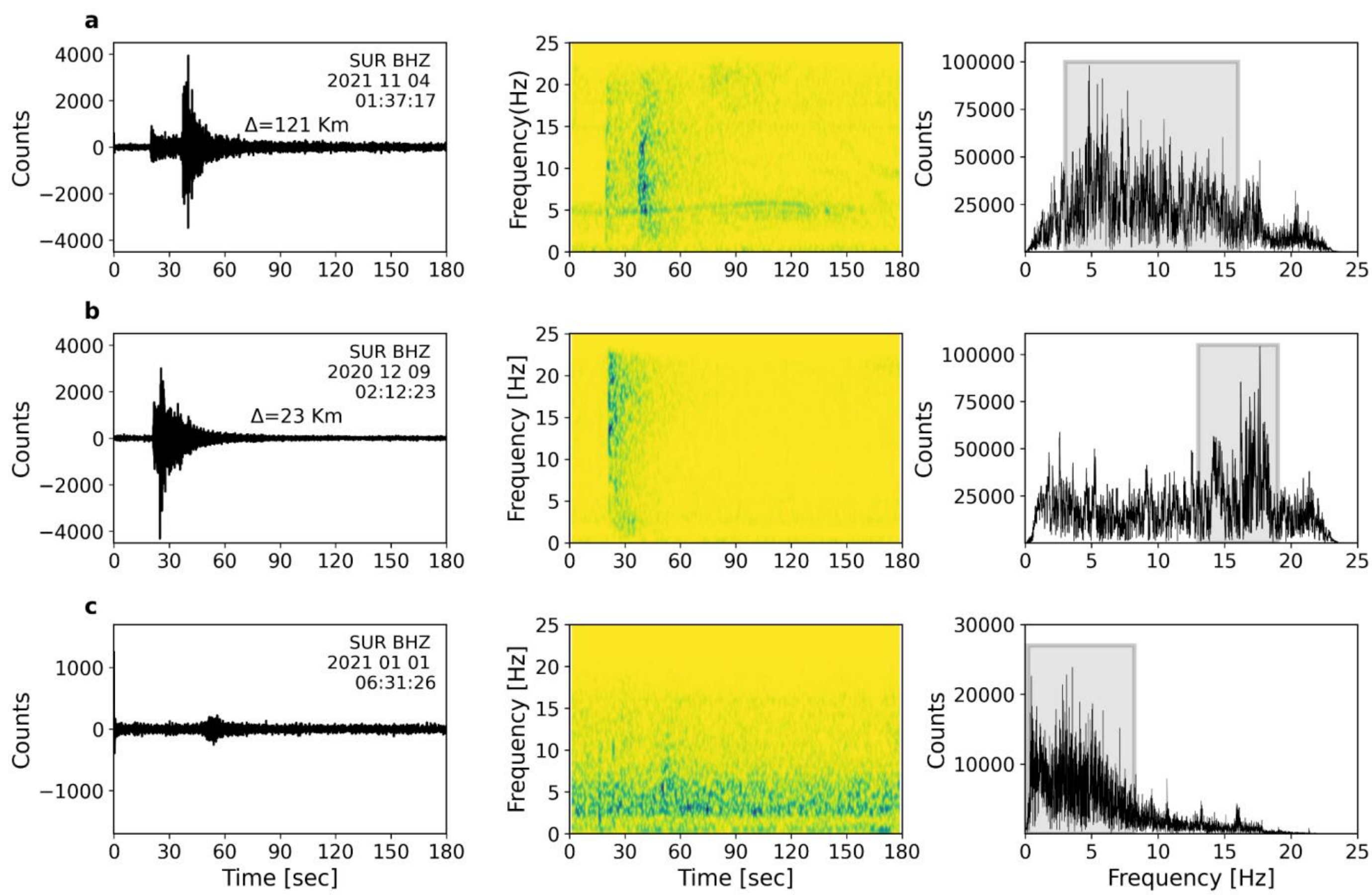

Figure 2: Examples of (A) an earthquake, (B) a blast, and (C) noise recorded at the SUR station. The station code, the component, epicentral distance (Δ) in kilometers, and the start time (UTC) of the chosen window are mentioned in the right corner of each waveform. The distinct spectral characteristics of each example can be seen in the corresponding frequency distribution (spectrogram) and frequency and amplitude distribution. Earthquake spectra exhibit two distinct frequency peaks corresponding to P- and S-phase arrivals, with predominant frequencies in the range of 3–16 Hz. Blast spectra show a single peak corresponding to the onset of the P-phase and have larger amplitudes in the higher frequencies between 12 and 18 Hz. Seismic noise amplitudes are generally lower and in the frequency range less than 5 Hz.

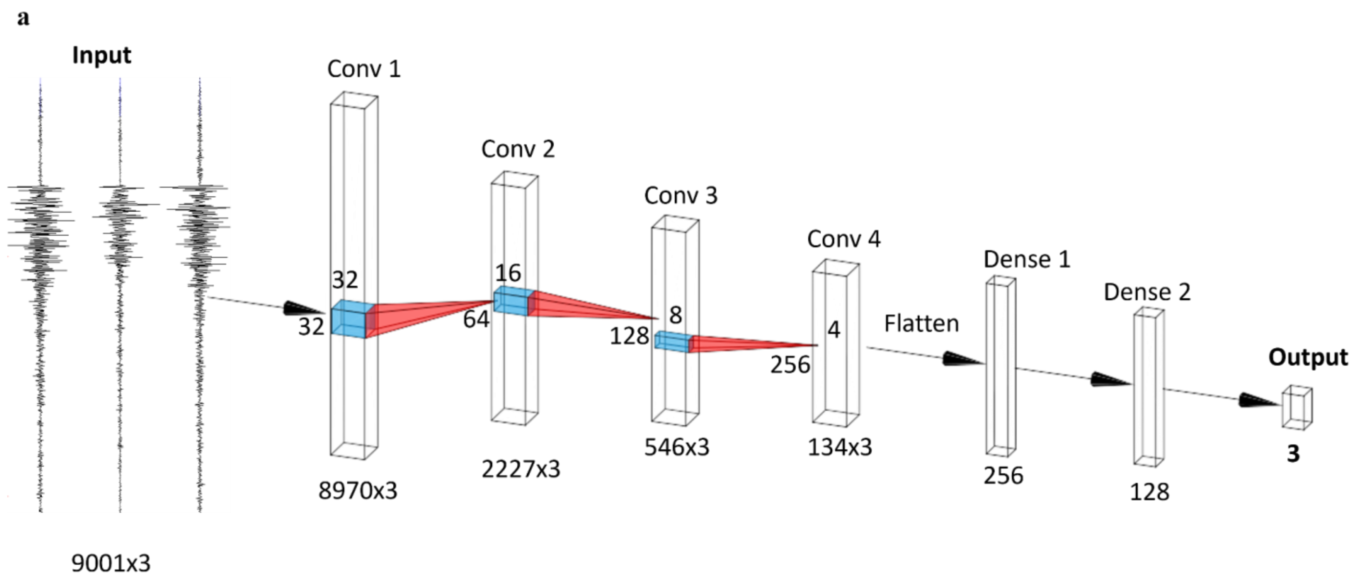

Figure 3(a): Schematic representation of the waveform-based CNN model's architecture developed in this study to discriminate between earthquakes, blasts, and seismic noise. The input for this model is a three-channel waveform of 180 seconds length at a sampling rate of 50 Hz. The input shape is (9001,3) corresponding to the number of points, and channels. This model was built with 4 1D CNN layers, with SeLU activation function. The output dimension is provided below each layer before the final prediction of the three classes (earthquakes, blasts, and seismic noise) using the softmax activation function.

b

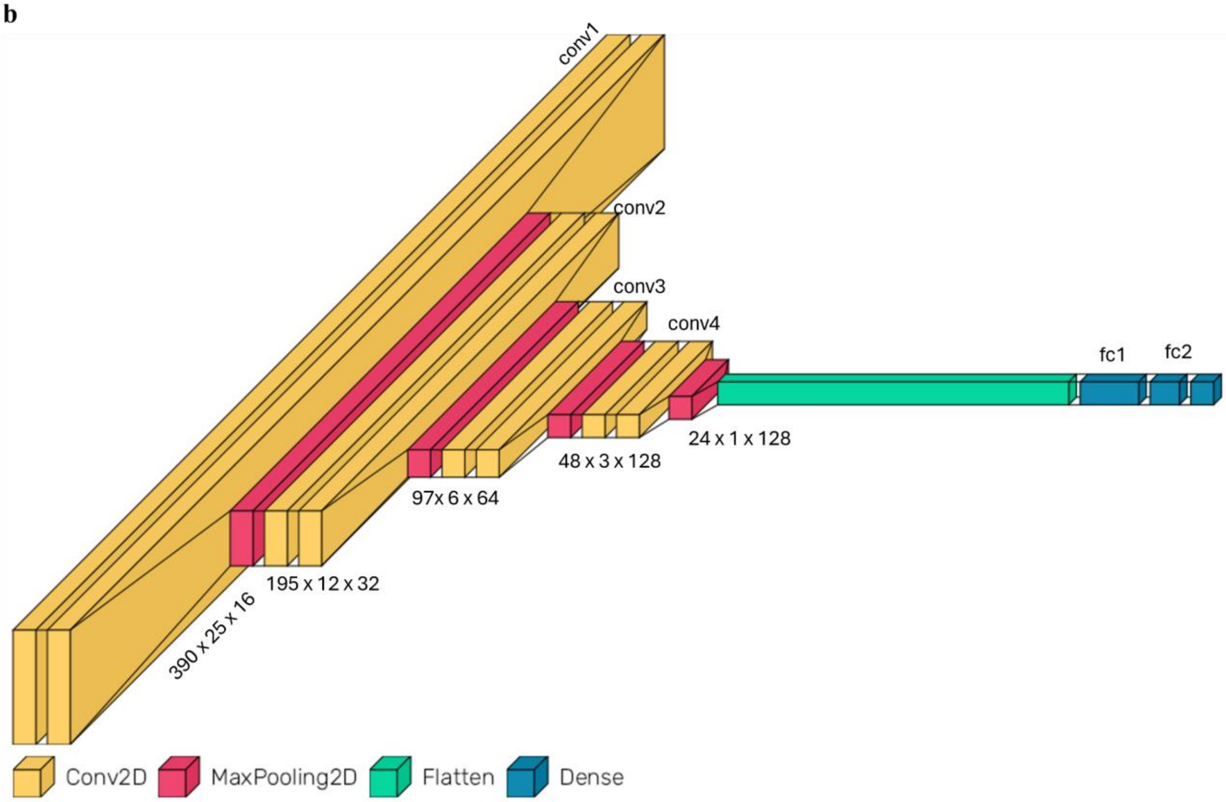

Figure 3(b): Schematic representation of the spectrum-based CNN model's architecture developed in this study to discriminate between earthquakes, blasts, and seismic noise. The input for this model is a three-channel spectrogram of 180 seconds length at a sampling rate of 50 Hz. The input shape is (390,25,3) corresponding to the number of points, frequency, and channels. The yellow block represents the 2D CNN layers which uses SeLU activation function followed by 2D MaxPooling layers (red blocks) which reduces the dimension of the input data from 390 to 24 before flattening the data for fully connected layers that will be used for the final prediction of the three classes of earthquakes, blasts, and seismic noise using the softmax activation function.

Figure1(a).

a

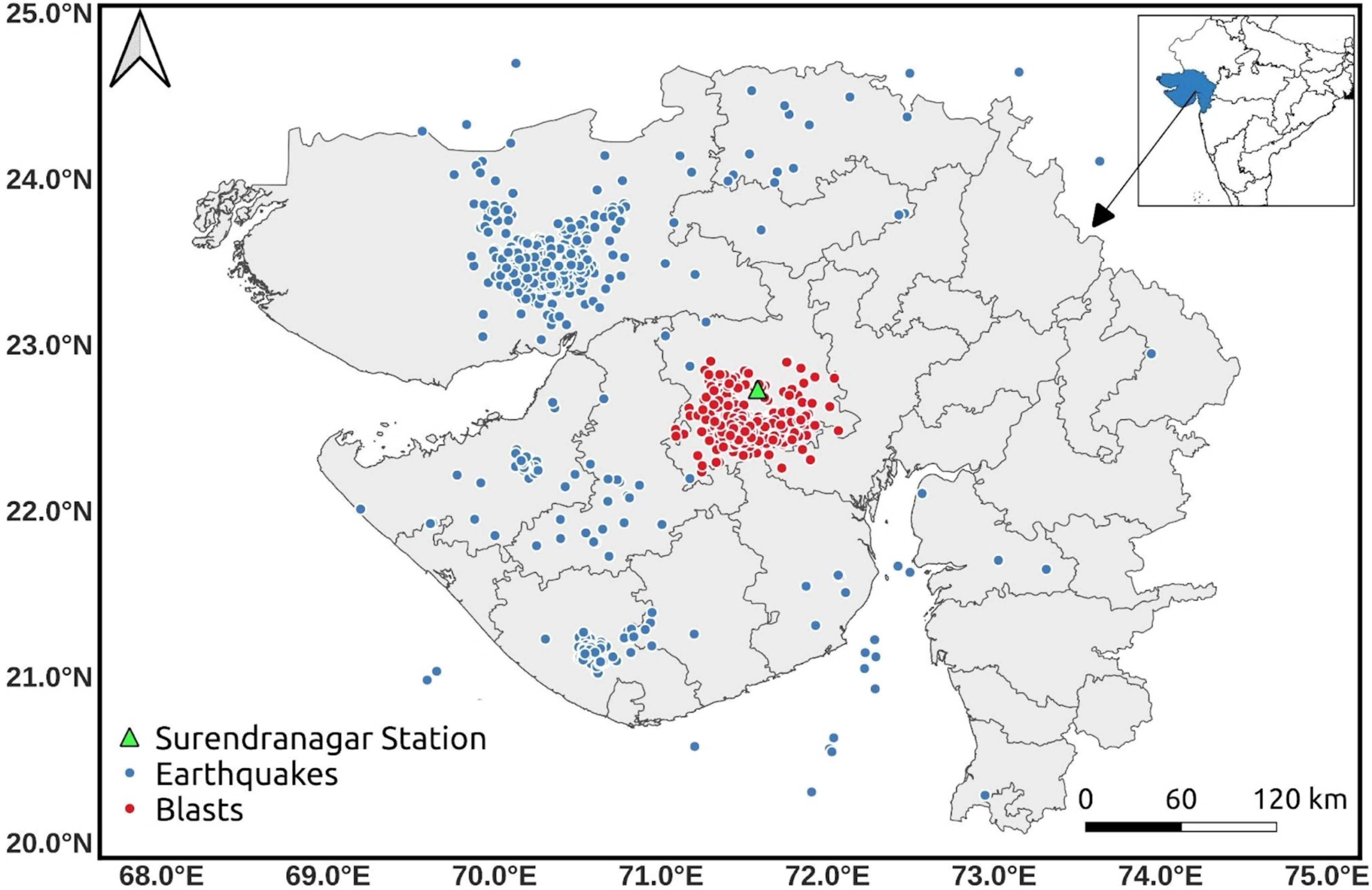
25.0°N
24.0°N
23.0°N
22.0°N
21.0°N
20.0°N
68.0°E
69.0°E
70.0°E
71.0°E
72.0°E
73.0°E
74.0°E
75.0°E
Surendranagar Station
Earthquakes
Blasts
0
60
120 km

Figure1(b).

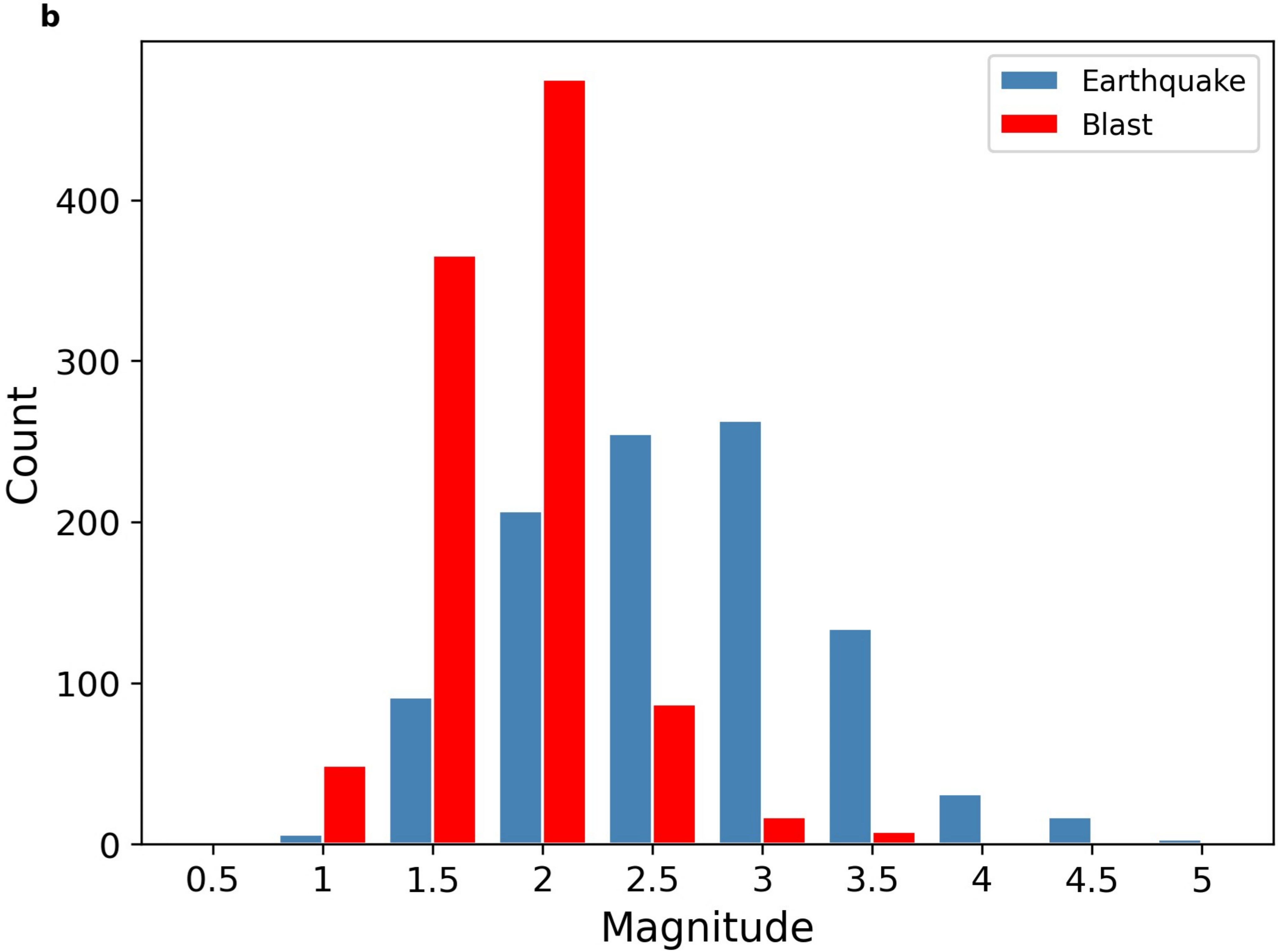
b
Earthquake
Blast
Count
0
100
200
300
400
0.5
1
1.5
2
2.5
3
3.5
4
4.5
5
Magnitude

Figure2.

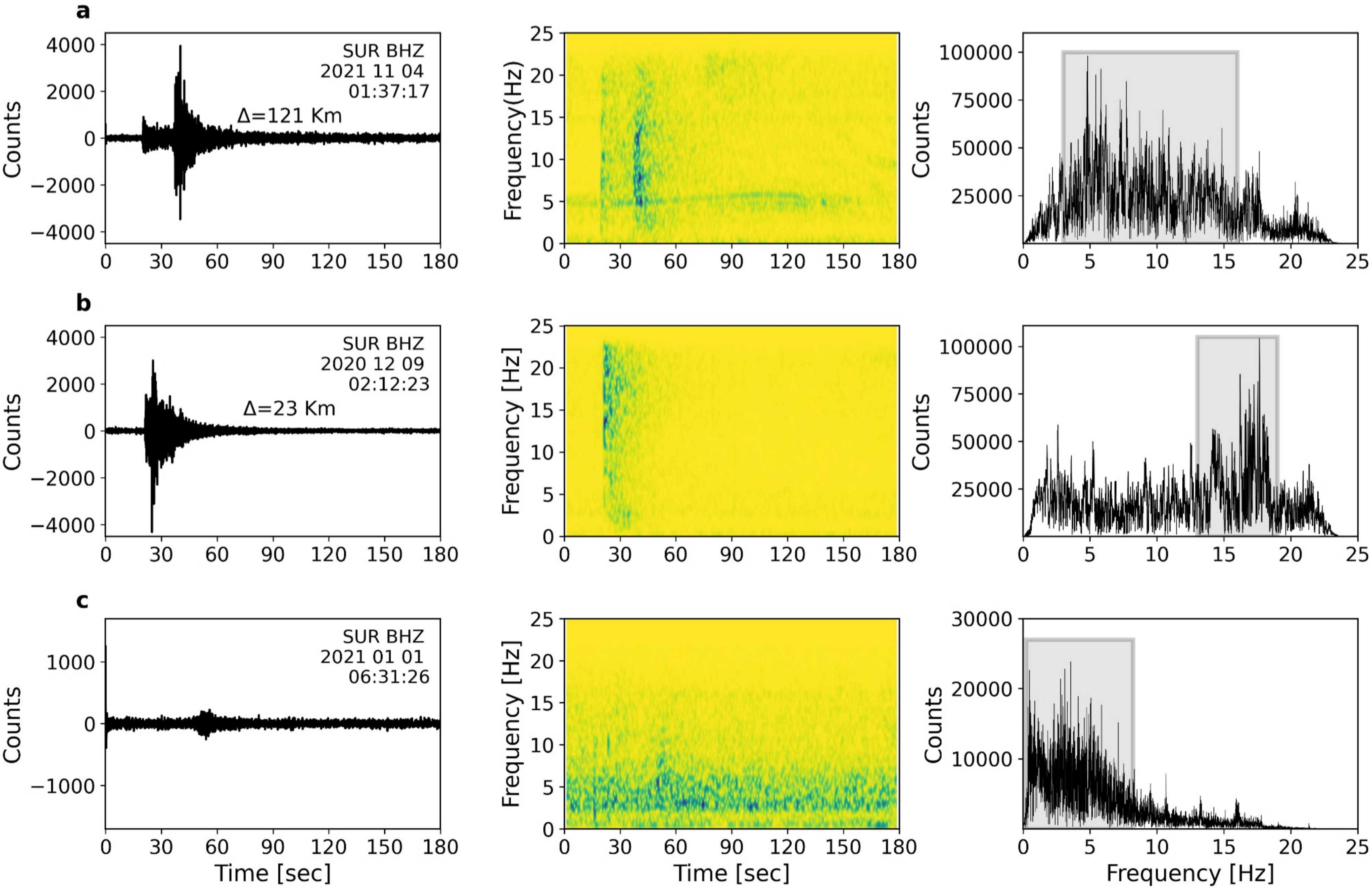
a
SUR BHZ
2021 11 04
01:37:17
Δ=121 Km
Counts
Frequency(Hz)
Counts
b
SUR BHZ
2020 12 09
02:12:23
Δ=23 Km
Counts
Frequency [Hz]
Counts
c
SUR BHZ
2021 01 01
06:31:26
Counts
Frequency [Hz]
Counts
Time [sec]
Time [sec]
Frequency [Hz]

Figure3(a).

a

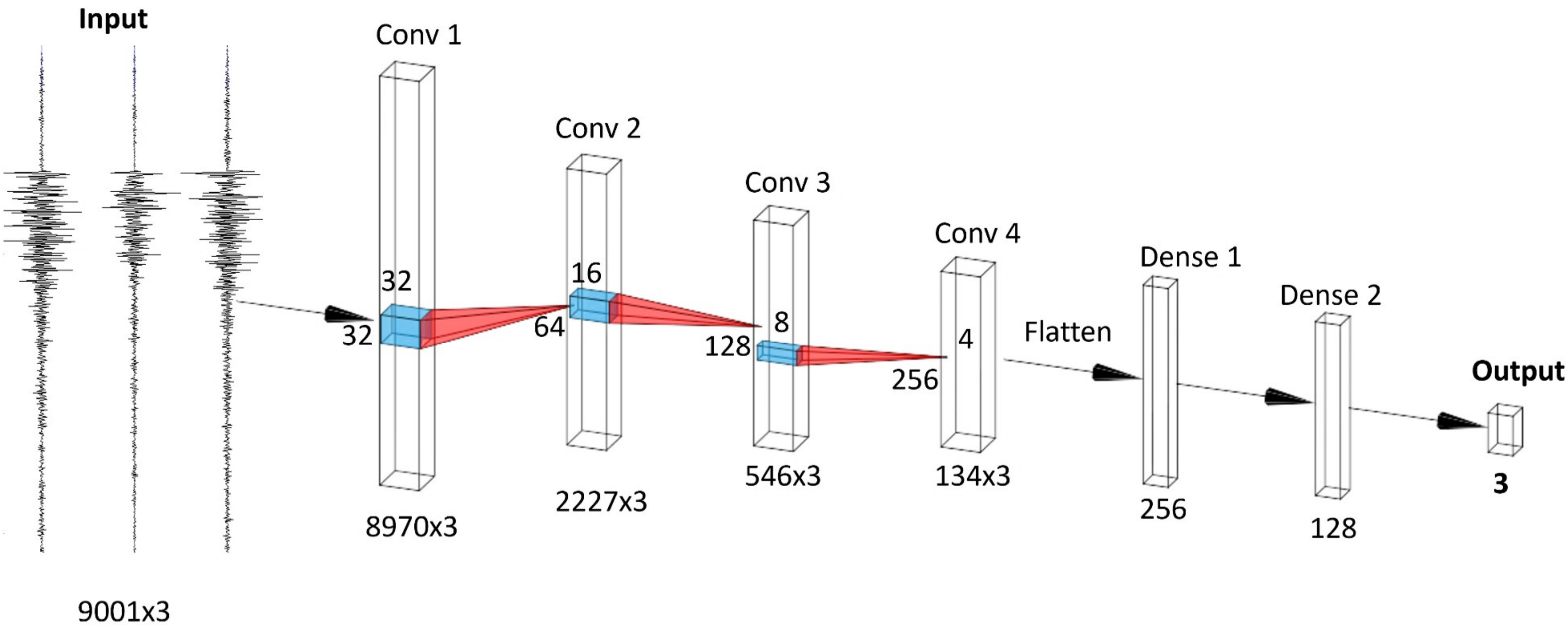

Input
9001x3
Conv 1
32
32
8970x3
Conv 2
16
64
2227x3
Conv 3
8
128
546x3
Conv 4
4
256
134x3
Flatten
Dense 1
256
Dense 2
128
Output
3

Figure3(b).

b

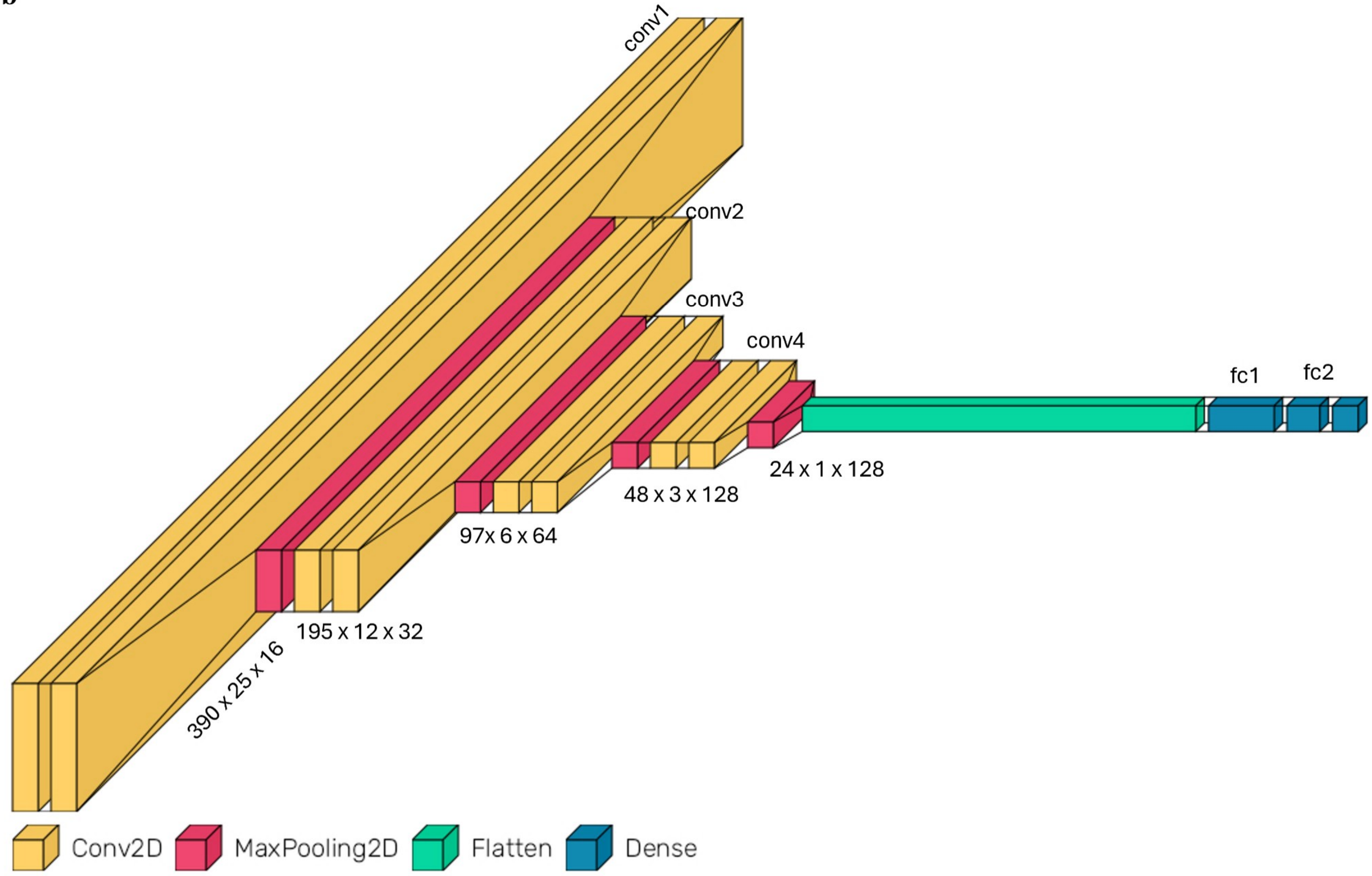
conv1
conv2
conv3
conv4
fc1
fc2
390 x 25 x 16
195 x 12 x 32
97x 6 x 64
48 x 3 x 128
24 x 1 x 128
Conv2D
MaxPooling2D
Flatten
Dense

Table 1: Summary of the evaluation parameters obtained for waveform (WF), spectrum (SPEC) and combined (COM) models.

Classes	**F1 Score**			**Recall**			**Precision**		
	WF	SPEC	COM	WF	SPEC	COM	WF	SPEC	COM
Earthquake	0.91	0.95	0.95	0.92	0.97	0.94	0.97	0.94	0.96
Blasts	0.93	0.92	0.93	0.95	0.89	0.92	0.91	0.96	0.93
Noise	0.98	0.97	0.98	0.99	0.98	0.99	0.97	0.96	0.96

Application of Deep Learning to Seismic Event Classification in the Gujarat Region, India

D. Pragnath [1,3], G. Srijayanthi [1], *, Johannes Faber[2,4], Jonas Köhler[2,4], Wei Li[2], Nishtha Srivatsava [2,4], Santosh Kumar [1], Sumer Chopra [1]

[1] Institute of Seismological Research, Gandhinagar, Gujarat, India

[2] Frankfurt Institute for Advanced Studies, Frankfurt, Germany

[3] Gujarat University, Ahmedabad, Gujarat, India

[4] Goethe Universität, Frankfurt am Main, Germany

*srijayanthi.india@gmail.com

Key Points

- Developed 3 CNN models to classify blasts, earthquakes & noise based on the features extracted from waveform, spectrum & combining both.
- All 3 models have >93% accuracies and exhibit exceeding performance in matrix scores F1, recall and precision.
- These models produce > 90% accuracies when tested on new datasets from SCEDC and Palitana region Gujarat.

Abstract

In anticipation to substitute the existing manual/semi-automated methods for classifying quarry blasts, earthquakes, and noise, we developed three convolutional neural network (CNN) models. The three CNN models extract relevant features from seismograms (waveform), spectrograms (spectrum), and a combination of the two respectively. A total of 3414 samples were extracted from the three categories, 15% of the data from each category were split for testing, and the remaining data were augmented and used for training. The waveform model, spectrogram model, and combined model achieved accuracies of 95.32%, 93.13%, and 93.96%, respectively. The reliability of these models was ascertained by promising accuracies of >90% and 100% obtained for large and small datasets from testing with SCEDC data and records from the Palitana region (Gujarat) respectively. The results of this study demonstrate the potential of deep learning-based approaches for the effective classification of seismic events.

Key Words: Deep Learning, CNN, Earthquakes, Quarry blasts, Noise, Spectrogram, Gujarat.

1. INTRODUCTION

Seismicity monitoring is one of the primary objectives in traditional seismological studies. This process requires manual inspection, which is time-consuming and is often associated with errors and biases. Continuous seismic networks used for monitoring seismicity at local and regional scales are thus contaminated with events other than natural earthquakes (Linville et al., 2019). Therefore, discriminating between a local tectonic event and a mining or quarry blast is a routine yet challenging task for both researchers who compile earthquake catalogs and those monitoring seismic networks (Astiz et al., 2014). Further, identification of blasts and earthquakes becomes especially challenging in near real-time monitoring when both the tectonic earthquakes and anthropogenic sources are in proximity (Whidden & Pankow 2012; Wiemer & Baer 2000; Horasan et al., 2009) and the earthquake location has to be reported in less than 10 minutes of earthquake occurrence.

Traditional seismological methods include manual, semi-automated and automated methods to discriminate between tectonic earthquakes, blasts and noise. Initially, the identification was based on occurrence time and location, often represented by the day-night distribution plot. Explosions usually occur during working hours from the same location, unlike earthquakes that can happen at any time and from any location. Later, more technical discrimination techniques were adopted based on waveform and spectrum analysis, such as ratios of amplitudes of various seismic phases (Bennett & Murphy 1986; Wüster et al., 1993; Anderson et al., 2009; Mc Laughlin et al., 2004), velocity spectra assessment (Taylor et al., 1988; Kim et al., 1994; Gitterman et al., 1998; Walter et al., 1995), ratios of corner frequencies (Korrat et al., 2022) and power spectral densities (Sertcelik et al., 2020). For large magnitude earthquakes (M>4), even the moment tensor solutions can be used for identifying the source. However, all these methods may not be applicable in all scenarios and are restricted by magnitude, distance and the type of instrument used to record these seismic signals. Moreover, manual methods are time consuming, require substantial effort for data selection, extraction, conversion and computation of the parameters and subsequent labeling of seismic events as blasts, earthquakes and noise. Unlike certain selection criteria such as window length for estimating amplitude, spectra, or magnitude, choosing corner frequencies and appropriate methods require individual experience and knowledge to ensure the correctness of the obtained results, which can vary for different scenarios. This can lead to partial loss of information or subjective factors affecting the outcome.

Machine learning based classification models can overcome these challenges by preserving all parameter information based on the original waveform data and avoiding the impact of subjective experience on classification outcomes. The advent of machine learning (ML) techniques has significantly impacted various scientific disciplines, including seismology, leading to numerous publications on ML and deep learning-based models for seismic signal classification (Renouard et al., 2021; Linville et al., 2019; Saad et al., 2019, 2022; Li et al., 2022). In the present study, three CNN architectures were developed to identify earthquakes, quarry blasts and seismic noise. The first architecture is based on waveform analysis, the second on spectrum analysis, and the third on a combination of both waveform and spectrum features. The accuracies of all the three models were ≥ 93%.

2. DATA

2.1 Data collection

The Gujarat State Seismic Network (GSNet), operated by the Institute of Seismological Research (ISR), Gandhinagar, has been well-maintained since July 2006 (Chopra et al., 2008). The network consists of 60 Broadband Seismograph Stations (BBS) spread throughout the state and neighboring areas. Data from 45 BBS were transmitted to the Institute of Seismological Research via VSAT, enabling near real-time (24 × 7) monitoring of earthquake activity. Over the years, the network has recorded a significant number of earthquakes, primarily from Kachchh, Saurashtra, and mainland regions of Gujarat state (Rastogi et al., 2013). ISR is also obligated to promptly provide a preliminary earthquake report of all the earthquakes with magnitudes M≥2.5. These reports should be transmitted within minutes of the earthquake occurrence to both the disaster management authorities and state emergency response center through various modes of communication like email, SMS and the web. A recent study by Kumar et al., (2021) indicated an increase in low-magnitude earthquakes in the past decade, clustering mainly near Surendranagar region in the Saurashtra peninsula and Godhra in the mainland regions, predominantly during daytime (IST). These events were associated with high b-values and were initially suspected to be quarry blasts; this anticipation was later confirmed during the Corona lockdown period. Consequently, the identification of such quarry blasts in the seismic catalog is crucial to provide an earthquake catalog devoid of artificial/anthropogenic events.

In the present study, to differentiate earthquakes, quarry blasts and seismic noise, we utilized the waveform data recorded at Surendranagar (SUR) station from 2007 to 2022. The SUR station (71.580 N, 22.730 E) was chosen as it is a permanently established long-running station of GSNet and also has clear records of anthropogenic activities. The station was equipped with a CMG-3T seismometer, configured at 50 Hz. We identified a total of 1298 blasts, which were ~25 to 37 km from the SUR station, within a region associated with mining-related quarries (Kumar et al., 2021) (Figure 1a). The magnitude range of these blasts (~M 0.6 to M 3.5) closely matches the range of micro earthquakes. Additionally, we selected 1005 local earthquake waveforms with epicentral distances ranging from 30 km to 110 km across Gujarat in the magnitude range of M 0.7 to M 4.5. The earthquakes were carefully chosen with a considerable overlap in the lower magnitude range to have comparable waveforms in the lower magnitude range as in the blast's dataset. To create a uniform dataset of seismic noise, we randomly selected 1111 noise samples encompassing different times of the day and seasons throughout the year. This approach ensures that the dataset represents all possible noise scenarios over different times, seasons and years. The magnitude distribution of the blasts and earthquakes used in the present study were shown in Figure 1b.

Seismological waveform data are a conglomeration of multiple factors like nature of the source, epicentral distance, the travel path/medium and the station location or the underlying geology that mostly influences the noise characteristics. The quality of waveforms (clear seismic phases) also hugely depends on the magnitude as well. It is a challenging job to identify clear phases in the case of lower magnitudes where the energy quickly attenuates resulting in low signal to noise ratio and weak phases that can hardly surpass the background noise level (Korrat et al., 2022; Tibi et al., 2019). Considering all the above-mentioned factors, we employed a 180 s window length for earthquakes, blasts, and noise unlike other published models (Liu et al., 2021; Kong et al., 2022) that utilized ≤ 100s window length. The longer waveform length was chosen to preserve features such as coda length, which differs significantly between earthquakes and blasts, especially for earthquakes with large magnitudes and epicentral distances, resulting in longer coda lengths.

Each earthquake and blast were manually verified and visually inspected based on occurrence time (7 am to 7 pm IST), geographical location, and waveform characteristics, including coda length and P, S phase amplitudes. Furthermore, we observed that identifying the source characteristics is much simpler in the frequency domain than in the time domain (Korrat et al., 2022), as the spectrogram illustrates the signal intensity across different frequencies found within an arbitrary waveform. We plotted spectrograms that provided a clear identification of the source, particularly when categorizing events in the lower magnitude range with low signal-to-noise ratios (Allmann et al., 2008). The spectrum of earthquakes exhibited two distinct frequency bands corresponding to P and S phases in the chosen window length (Figure 2a). Conversely, the spectrum of blasts showed a single band corresponding to the onset of the P phase (Figure 2b). An example of the seismic noise spectrum is shown in Figure 2c. Therefore, a total of 3414 waveforms that include 1298 blasts, 1005 earthquakes and 1111 noise samples were labeled for further processing.

2.2 Data pre-processing and splitting

The most commonly observed issue in seismic waveforms is that traces deviate from the baseline and are associated with some long periodic trend (Liu et al., 2021). Therefore, all the waveforms are corrected for the trend and mean using detrend and demean tools in ObsPy (Breckpot et al., 2010; Krischer et al., 2015). As the first step in deep learning a test dataset, comprising 15% of the raw/unaugmented data, was separated. This test dataset was not used to train the model, and its purpose was to assess the statistical significance of the model's performance. The test set consists of 513 seismic events, almost equally weighted among the three classes; earthquakes (151), blasts (195) and noise (167). The same test dataset was used for all the three models, namely the waveform, spectrum and combined model.

2.3 Data Augmentation

The crux of deep learning models largely depends on the quality, quantity, and consistency of the labeled dataset used for training. Therefore, a limitation of machine learning is the lack of sufficient amount of training data or uneven class balance in a dataset. The present objective for the 3-class classification requires a huge dataset, but the dataset consists of 2901 waveforms which is insufficient for deep learning. So, we adopted the technique of data augmentation to overcome this limitation and construct a suitable training dataset using ObsPy. The data is augmented by: (i) flipping the polarities of the waveforms, (ii) applying bandpass filter from 2.0 Hz to 8.0 Hz and, (iii) randomly muting one trace. The miniseed files are converted into Numpy (Harris et al., 2020) arrays and are saved in '.npy' format with a shape of (9001, 3), where 9001 represents the 'npts' (number of points) and 3 represents the number of channels. In order to maintain uniform trace length or equal number of 'npts', the traces with shorter lengths were padded with zeros at the end. This resulted in a total of 11,614 waveforms that were used as training dataset for the waveform model.

The spectra are computed for the raw waveforms after correcting for the trend and mean. The data augmentation in waveforms shows noticeable changes especially when the polarities of the waveform were flipped. However, such differences/changes were not visually identifiable in the spectrograms. Therefore, the spectrum data of the earthquakes, blasts and noise were augmented by applying band-pass (2.0-8.0 Hz), low-pass (8.0 Hz), and high-pass (2.0 Hz) filters. The input shape for the spectrum model was (390, 25, 3), corresponding to (time × frequency × channels). To maintain the same shape, zero padding was applied at the end of the spectrum data.

3 CNN MODELS

Recent studies have highlighted the effectiveness of CNN-based identification methods in seismic data processing and the extraction of characteristic features. These features can aid in discrimination and classification based on pixel-level information, thereby synthesizing global information. In the present study, we developed three CNN models based on waveforms, spectrograms and combined parameters to classify local earthquakes, quarry blasts and seismic noise. To build these models, TensorFlow (Abadi, 2016) was utilized and all the three models were trained on the Nvidia RTX A5000. Each of these models were described below. All the models were trained on the data recorded at a single station SUR.

A Categorical Cross-Entropy loss function and an Adam optimization method (Kingma et al., 2014) were used to train all the models below. To prevent our models from overfitting data, we incorporated an early stopping mechanism. This means that if the accuracy remains unchanged for selected consecutive epochs (which can be defined through the parameter called “patience"), the training process terminates. This approach ensures the reliability of the training process. In the present study, we chose patience as 10 for all the three models.

3.1 Waveform Model

For training the waveform CNN model, three-component seismogram data with a length of 180s (20s before and 160s after the first arrival) was utilized. For distinguishing the three classes (earthquakes, quarry blasts and noise) we developed a 4 layered convolutional model with filter counts 32, 64, 128 and 256. The model has two fully connected (FC) layers (256, 128) with max-pooling and drop-out layers between each layer show in Figure 3(a). The probability of each class was computed from the output layer using the 'softmax' activation function (Nwankpa et al., 2018). The best accuracy of 95.32 % was obtained with a learning rate of $2*10^{-4}$ and a batch size of 16 given in Table S1 in of Supporting Information.

3.2 Spectrum Model

This model was developed as an alternative approach to discriminate earthquakes and quarry blasts based on spectrograms. Extracting information from spectrograms provides a reliable classification. The spectrograms show clear distinguishing features that can be used to train the model for reliable classification, even in the low-to-intermediate magnitude range of earthquakes and quarry blasts. The spectrograms are computed for 1s sliding windows with 50% overlap, which results in 390-time windows for which we compute the discrete Fourier transform between 1 and 25 Hz for the three components of the seismogram each having 180 s data length. Thus, the spectrogram's model input size is (390 × 25 × 3). Spectrum model focuses on different frequency bands generated due to the arrival of different phases (P and S) to make the three-class identification. This model consists of 4 convolution layers with 16, 32, 64 and 128 filters, and two fully connected layers at the end. We applied a 2 × 2 'max-pooling' between each convolution layer and the final layer is the fully connected output layer that computes the probabilities obtained for different classes using the 'softmax' activation function shown in Figure 3(b). The activation function used for this model is SeLU and an accuracy of 93.13% is obtained.

3.3 Combined Model

The combined model was developed combining the architectures of waveform and spectrogram models incorporating the features from both waveform and spectrum. The features thus extracted from both the models are then combined with a concatenation layer. The concatenated features are then passed through a FC layer before the model predicts the final classification shown in Figure S1. The SeLU activation function was used across the network appended by a last layer of softmax activation function with three neutrons for a 3-category classification problem. An accuracy of 93.96 % was obtained using this model.

4. RESULTS AND DISCUSSION

In this study, we employed a training dataset comprising 11,614 waveforms and a test dataset of 513 waveforms to build three models namely waveform, spectrogram and combined. The achieved accuracies for these models were 95.32%, 93.13%, and 93.96%, respectively. Further, the performance of these models were assessed using Receiver Operating Characteristic (ROC) curves on the test dataset. These curves are useful for testing the model's ability to classify input by plotting the true positive rate against the false positive rate. The Area Under the Curve (AUC) was employed as a metric to measure the quality of the ROC curve, with a value of 1 signifying optimal performance (Figure S2), the AUC values of each model with individual class values are given in Table S2. The AUCs are >0.97 for each model indicating the model's ability to correctly distinguish various classes (Table S2)

In ML, to evaluate the performance of a classification of models these four parameters are used namely, accuracy (Acc), precision (Pr), recall (Re) and F1-score (F1).

$$Acc = \frac{TP + TN}{FP + TP + TN + FN} \quad (1)$$

$$Pr = \frac{TP}{TP + FP} \quad (2)$$

$$Re = \frac{TP}{TP + FN} \quad (3)$$

$$F1 = 2\ \frac{Re * Pr}{Re + Pr} \quad (4)$$

where, TP and TN are abbreviations for True Positive and True Negative, similar to FP and FN, which represent False Positive and False Negative. Accuracy (1) describes the correctness rate of the predicted labels, as it is the ratio of the sum of all the true predictions to the number of all possible predictions. The precision (2) value provides insights into TP (such as earthquake, blast, or noise in our case), where a value close to 1 indicates that most predictions are correctly identified. Recall (3) is the ratio of positively identified predictions to the number of actual positive classes. Thus, a higher recall value suggests that most predictions are correct, reducing the possibility of misclassification or false classification. The F1-score (4), unlike its counterparts recall and precision, considers both true and false predictions and is a weighted average of precision and recall. These parameters are calculated for each model and tabulated in table T1. These four parameters are >0.90 in all the three models. The precision value obtained from the waveform model is highest (0.97) for noise and earthquakes, indicating that these classes are better or correctly identified compared to the blasts that have least precision value (0.91). However, in the spectrum model, the ability to predict the blasts improves, indicating an increase in precision value (0.96) compared to the waveform model. Further, the confusion matrix provides detailed insights on the actual number of true and predicted classes in each category. The confusion matrix of the three models (Figure S3) shows the edge of each model over the other. Although the waveform model gives best predictions in all the categories, the combined model gives 100% correct prediction in the noise class. The same was expected from the spectrum model that was developed based on the difference observed in the predominant frequencies of blasts, noise and earthquakes (Figure 2). However, it failed to produce the expected outcome.

The waveform model produces the highest accuracy when compared to other models developed in the present study, and its performance is also comparable with the previously published waveform-based CNN model (Liu et al., 2021) to distinguish tectonic and non-tectonic earthquakes. Their model was trained and tested using data from the China Earthquake Network Center. They obtained an accuracy of 92% with their four layered model using the Rectified Linear Unit (ReLU) activation function in a 7-layered CNN model. In another study, Hourcade et al. (2022) developed a 4-layered spectrum-based CNN model with the ReLU activation function. There model was trained to differentiate between natural and anthropogenic events from metropolitan France, and it achieved an accuracy of 98%.

4.1 Misclassifications by Waveform-based CNN

The waveform-based model identifies noise with high accuracy (99%). However, a small proportion of the test set (4%, comprising 22 waveforms) was misclassified, primarily consisting of blasts and earthquakes. A visual examination of the misclassified waveforms was conducted (Figure S4) to identify any specific patterns or features that are contributing to the misclassification of certain waveforms. Subsequently, the signal-to-noise ratio (SNR) was also calculated using the following formula to quantify the limitations of the waveform-based model with respect to the relative strength of the seismic signal to the background noise.

$$SNR = 10\, log_{10}\left(\frac{\mu\, S^2}{\mu\, N^2}\right) \qquad (5)$$

where, $\mu\, S^2$ represents the mean squared amplitude of the seismic signal calculated over a 10 s interval post the first arrival, and $\mu\, N^2$ represents the mean squared amplitude of background noise calculated over a 10 s interval preceding the first arrival (Figure S5).

The resulting SNR value, expressed in decibels (dB), provides a measure of the relative strength of the seismic signal to the background noise. In the present study the SNR varies from -9 to 44 dB (Figure S6). The negative values are obtained when the ratio of $\left(\frac{\mu\, S^2}{\mu\, N^2}\right)$ is < 1 which indicates that the noise dominates over the signal. $\left(\frac{\mu\, S^2}{\mu\, N^2}\right)$=1 means that the strength of signal and noise are equal, resulting in a SNR of 0 (as $10\ log_{10}$ (1) = 0). Majority of the misclassified waveforms (15 i.e. 68% of the total misclassified waveforms) have low SNR <10 (Figure S6 (c)) and ≥ 50% prediction probability for the wrong class given in Figure S7.

4.2 Misclassification by Spectrogram-based CNN

A clear distinction between an earthquake and a quarry blast was evident on a spectrogram (Figure 2), prompting us to develop a spectrum-based model to improve the accuracy of classification. Although the spectrum model achieved good classification results, they were not as promising as anticipated. Visual inspection of the misclassified spectrogram records revealed two issues: (1) strong and consistent energy at a particular frequency band throughout the selected time window, and (2) a frequency response resembling a sinusoidal trend from an unidentified source (example shown in Figure S8). Attempts to mitigate these issues by applying a bandstop filter resulted in the loss of information and created a void at that particular frequency band (Figure S8(b)). An improved dataset would provide a more comprehensive understanding of the model's behavior and enhance its robustness, which is currently limited by the limited dataset.

5. INDEPENDENT TEST

The three models developed in the present study were mainly trained using GSNet data. However, to make sure they work well in different situations, we tested them using earthquake data from the Southern California Earthquake Data Center (SCEDC). A total of 1037 events were downloaded, with 417 earthquakes recorded at BJX station and 620 blasts recorded at EDW2 station. An accuracy of 94%, 90% and 91% was obtained with waveform model, spectrum and combined model respectively results were given in Fig S9.

Further, while preparing this manuscript, we observed some unexpected seismic activity from a region named Palitana, in the Gujarat state of India, hitherto devoid of any active seismic activity from previous GSNet monitoring for almost 16 years. Thus, we tested these few ambiguous waveforms, and with 100% certainty, these events were classified correctly as quarry blasts with all our three models.

6. CONCLUSION

In order to reduce the amount of processing time for classifying various seismic events, in the present study we developed three deep learning classification models based on waveform, spectrogram, and combining both utilizing the CNNs. These models identified seismic noise, quarry blasts, and earthquakes with an accuracy of 95.32%, 93.13%, and 93.96% respectively. To verify the dependability and efficacy of these models, tests were conducted on alternative datasets. This testing provided us clear evidence that these models can be effectively utilized for classification of seismic events (earthquakes & blasts) from other regions as well. The accuracy and application of our models to different regions can be further effectively improved by increasing our labelled dataset with varied examples.

The ML based approaches are more efficient and accurate in discriminating earthquakes and blasts over manual methods that are limited by magnitude and SNR. In the present study, 185 waveforms have SNR < 10, which means that the noise is dominant over the signal and only 15 (8% of 185 waveforms) were misclassified and 92% of the events were correctly classified, even in the low magnitude range and noisy data. The proposed classification models can improve the speed and accuracy in detecting the microseismic events and quarry blasts. This approach can be used to discriminate in real time and reduce the mislabelled/ambiguous events and thus constituting in making the catalog as reliable as possible. On a long-term basis we plan to use these models for monitoring illegal mining activity in Gujarat state as such activities demand attention from local governing bodies which may cause important implications for the safety and environmental management.

7. FUTURE WORK

These classification models will be further developed for near real time monitoring which includes phase detection and estimating the earthquake location parameters. This should be able to reduce the manual efforts to identify different sources and also estimate the location and magnitude within a fraction of seconds. Recent works utilized Fourier Neural Operators (Li et al., 2020; Sun et al., 2023) to develop near real time seismic monitoring. They proposed a model to identify the earthquakes and mark phases on the real time monitoring with multiple stations as input.

ACKNOWLEDGEMENTS

We acknowledge the support of the Department of Science and Technology, Government of Gujarat in establishing the broadband seismological network (GSNet) in Gujarat region. We would like to extend our sincere gratitude to FIAS for generously sharing their expertise in AI/ML. Their week-long course on AI/ML played a pivotal role in framing and guiding our work on this problem. Johannes Faber, Jonas Köhler, Wei Li and Nishtha Srivastava acknowledge the support by the Bundesministerium für Bildung und Forschung – BMBF for the “KI-Nachwuchswissenschaftlerinnen” – grant SAI 01IS20059

DATA AVAILABILITY

The data used in the study from Gujarat region (India), will be available on request to the Director General of the Institute of Seismological Research, Gandhinagar, Gujarat, India. The data used for testing (mentioned in section 5) can be downloaded from “https://scedc.caltech.edu/data/waveform.html”.

References

Abadi, M. 2016. TensorFlow: learning functions at scale. In Proceedings of the 21st ACM SIGPLAN international conference on functional programming, 1-1.

Allmann, B. P., Shearer, P. M., & Hauksson, E. (2008). Spectral discrimination between quarry blasts and earthquakes in southern California. Bulletin of the Seismological Society of America, 98(4), 2073-2079.

Anderson, D. N., Walter, W. R., Fagan, D. K., Mercier, T. M., & Taylor, S. R. (2009). Regional multistation discriminants: Magnitude, distance, and amplitude corrections, and sources of error. Bulletin of the Seismological Society of America, 99(2A), 794-808.

Astiz, L., Eakins, J. A., Martynov, V. G., Cox, T. A., Tytell, J., Reyes, J. C., ... & Vernon, F. L. (2014). The Array Network Facility seismic bulletin: Products and an unbiased view of United States seismicity. Seismological Research Letters, 85(3), 576-593.

Bennett, T. J., & Murphy, J. R. (1986). Analysis of seismic discrimination capabilities using regional data from western United States events. Bulletin of the Seismological Society of America, 76(4), 1069-1086.

Breckpot, R., & Marzec, M. K. (2010). ObsPy: a python toolbox for seismology, a data center perspective. Seismol. Res. Lett., 81(3), 530-533.

Chopra, S., Yadav, R. B. S., Patel, H., Kumar, S., Rao, K. M., Rastogi, B. K., ... & Srivastava, S. (2008). the gujarat (india) seismic network. Seismological Research Letters, 79(6), 806-815.

Gitterman, Y., Pinsky, V., & Shapira, A. (1998). Spectral classification methods in monitoring small local events by the Israel seismic network. Journal of seismology, 2, 237-256.

Harris, C. R., Millman, K. J., Van Der Walt, S. J., Gommers, R., Virtanen, P., Cournapeau, D., ... & Oliphant, T. E. (2020). Array programming with NumPy. Nature, 585(7825), 357-362.

Horasan, G., Güney, A. B., Küsmezer, A., Bekler, F., Öğütçü, Z., & Musaoğlu, N. (2009). Contamination of seismicity catalogs by quarry blasts: an example from Istanbul and its vicinity, northwestern Turkey. Journal of Asian Earth Sciences, 34(1), 90-99.

Hourcade, C., Bonnin, M., & Beucler, É. (2023). New CNN-based tool to discriminate anthropogenic from natural low magnitude seismic events. Geophysical Journal International, 232(3), 2119-2132.

Kim, W. Y., Simpson, D. W., & Richards, P. G. (1994). High-frequency spectra of regional phases from earthquakes and chemical explosions. Bulletin of the Seismological Society of America, 84(5), 1365-1386.

Kingma, D. P., & Ba, J. (2014). Adam: A method for stochastic optimization. arXiv preprint arXiv:1412.6980.

Kong, Q., Wang, R., Walter, W. R., Pyle, M., Koper, K., & Schmandt, B. (2022). Combining Deep Learning With Physics Based Features in Explosion-Earthquake Discrimination. Geophysical Research Letters, 49(13), e2022GL098645.

Korrat, I. M., Lethy, A., ElGabry, M. N., Hussein, H. M., & Othman, A. S. (2022). Discrimination between small earthquakes and quarry blasts in Egypt using spectral source characteristics. Pure and Applied Geophysics, 179(2), 599-618.

Krischer, L., Megies, T., Barsch, R., Beyreuther, M., Lecocq, T., Caudron, C., & Wassermann, J. (2015). ObsPy: A bridge for seismology into the scientific Python ecosystem. Computational Science & Discovery, 8(1), 014003.

Kumar, S., Kumar, R. C., Roy, K. S., & Chopra, S. (2021). Seismic monitoring in Gujarat, India, during 2020 coronavirus lockdown and lessons learned. Seismological Research Letters, 92(2A), 849-858.

Li, W., Chakraborty, M., Sha, Y., Zhou, K., Faber, J., Rümpker, G., ... & Srivastava, N. (2022). A study on small magnitude seismic phase identification using 1D deep residual neural network. Artificial Intelligence in Geosciences, 3, 115-122.

Li, Z., Kovachki, N., Azizzadenesheli, K., Liu, B., Bhattacharya, K., Stuart, A., & Anandkumar, A. (2020). Fourier neural operator for parametric partial differential equations. arXiv preprint arXiv:2010.08895.

Linville, L., Pankow, K., & Draelos, T. (2019). Deep learning models augment analyst decisions for event discrimination. Geophysical Research Letters, 46(7), 3643-3651.

Liu, X., Ren, T., Chen, H., & Chen, Y. (2021). Classification of tectonic and non-tectonic seismicity based on convolutional neural network. Geophysical Journal International, 224(1), 191-198.

McLaughlin, K. L., Bonner, J. L., & Barker, T. (2004). Seismic source mechanisms for quarry blasts: modelling observed Rayleigh and Love wave radiation patterns from a Texas quarry. Geophysical Journal International, 156(1), 79-93.

Nwankpa, C., Ijomah, W., Gachagan, A., & Marshall, S. (2018). Activation functions: Comparison of trends in practice and research for deep learning. arXiv preprint arXiv:1811.03378.

Rastogi, B. K., S. Kumar, and S. Aggarwal (2013). Seismicity of Gujarat, Nat. Hazards 65, no. 2, 1027–1044.

Renouard, A., Maggi, A., Grunberg, M., Doubre, C., & Hibert, C. (2021). Toward false event detection and quarry blast versus earthquake discrimination in an operational setting using semiautomated machine learning. Seismological Society of America, 92(6), 3725-3742.

Saad, O. M., Shalaby, A., & Sayed, M. S. (2019). Automatic discrimination of earthquakes and quarry blasts using wavelet filter bank and support vector machine. Journal of Seismology, 23, 357-371.

Saad, O. M., Soliman, M. S., Chen, Y., Amin, A. A., & Abdelhafiez, H. E. (2022). Discriminating earthquakes from quarry blasts using capsule neural network. IEEE Geoscience and Remote Sensing Letters, 19, 1-5.

SCEDC (2013): Southern California Earthquake Data Center. Caltech. Dataset. doi:10.7909/C3WD3xH1.

Sertçelik, F., Yavuz, E., Birdem, M., & Merter, G. (2020). Discrimination of the natural and artificial quakes in the Eastern Marmara Region, Turkey. Acta Geodaetica et Geophysica, 55, 645-665.

Sun, H., Ross, Z. E., Zhu, W., & Azizzadenesheli, K. (2023). Next-Generation Seismic Monitoring with Neural Operators. arXiv preprint arXiv:2305.03269.

Taylor, S. R., Sherman, N. W., & Denny, M. D. (1988). Spectral discrimination between NTS explosions and western United States earthquakes at regional distances. Bulletin of the Seismological Society of America, 78(4), 1563-1579.

Tibi, R., Linville, L., Young, C., & Brogan, R. (2019). Classification of local seismic events in the Utah region: A comparison of amplitude ratio methods with a spectrogram-based machine learning approach. Bulletin of the Seismological Society of America, 109(6), 2532-2544.

Walter, W. R., Mayeda, K. M., & Patton, H. J. (1995). Phase and spectral ratio discrimination between NTS earthquakes and explosions. Part I: Empirical observations. Bulletin of the Seismological Society of America, 85(4), 1050-1067.

Whidden, K. M., & Pankow, K. L. (2012). A catalog of regional moment tensors in Utah from 1998 to 2011. Seismological Research Letters, 83(5), 775-783.

Wiemer, S., & Baer, M. (2000). Mapping and removing quarry blast events from seismicity catalogs. Bulletin of the Seismological Society of America, 90(2), 525-530.

Wüster, J. (1993). Discrimination of chemical explosions and earthquakes in central Europe—a case study. Bulletin of the Seismological Society of America, 83(4), 1184-1212.

Tables and captions

Table 1: Summary of the evaluation parameters obtained for waveform (WF), spectrum (SPEC) and combined (COM) models.

Classes	**F1 Score**			**Recall**			**Precision**		
	WF	SPEC	COM	WF	SPEC	COM	WF	SPEC	COM
Earthquake	0.91	0.95	0.95	0.92	0.97	0.94	0.97	0.94	0.96
Blasts	0.93	0.92	0.93	0.95	0.89	0.92	0.91	0.96	0.93
Noise	0.98	0.97	0.98	0.99	0.98	0.99	0.97	0.96	0.96

Figures and Figure Captions

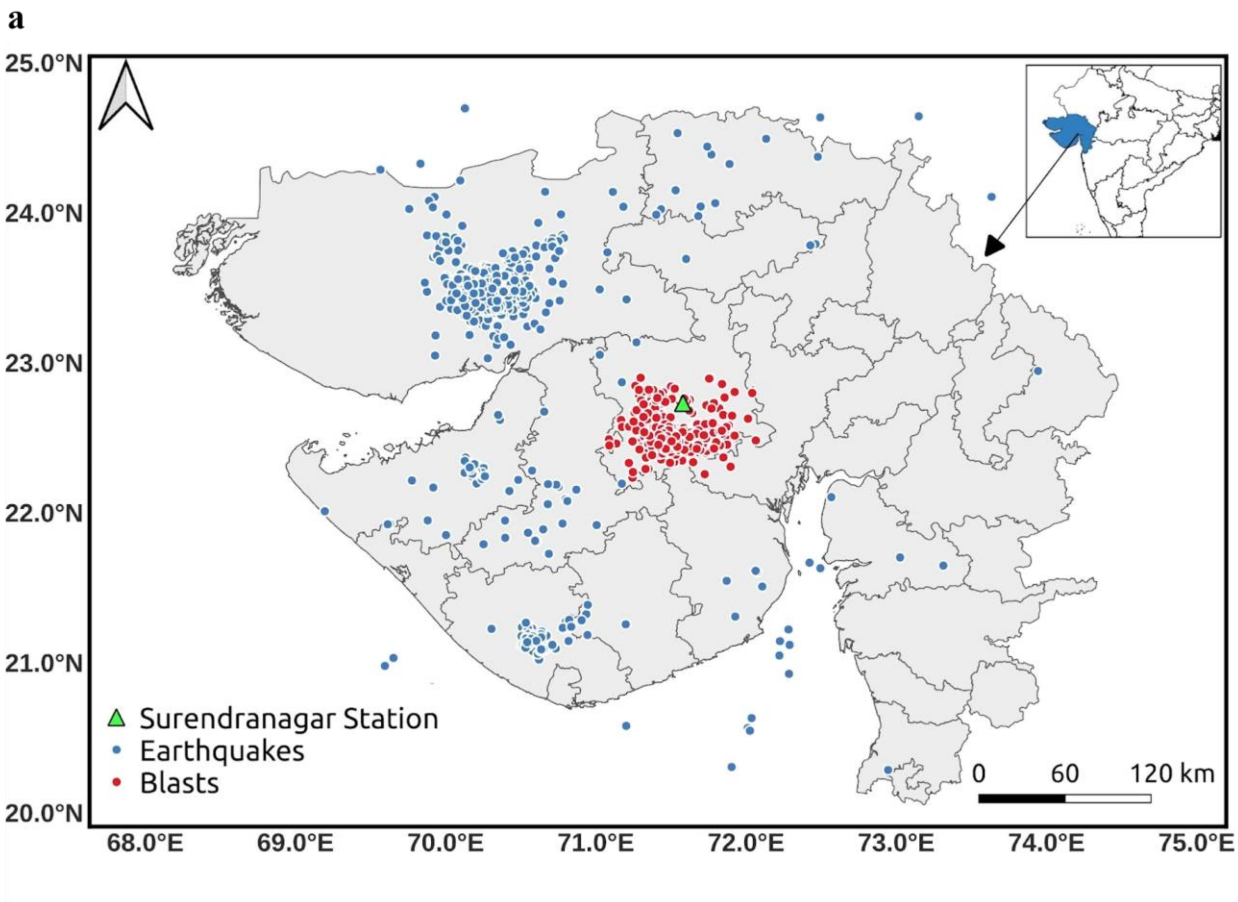

Figure 1(a): The spatial distribution of the earthquakes (blue circles) and blasts (red circles) used in the present study, recorded at Surendranagar (SUR) broadband station (green triangle). The inset map shows the Gujarat State in India.

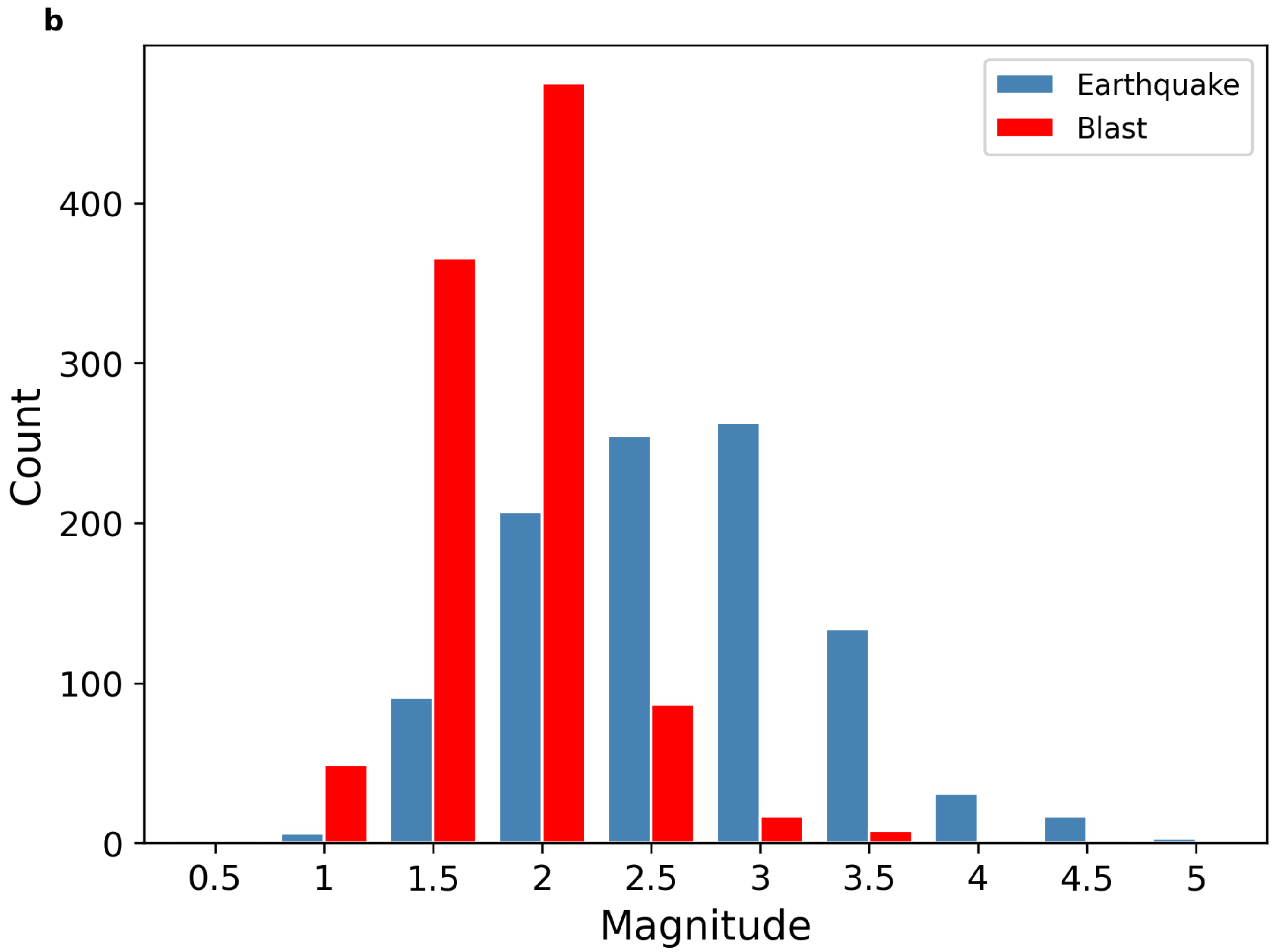

Figure 1(b): Magnitude distribution of the blasts and earthquakes (shown in figure 1) used in the present study.

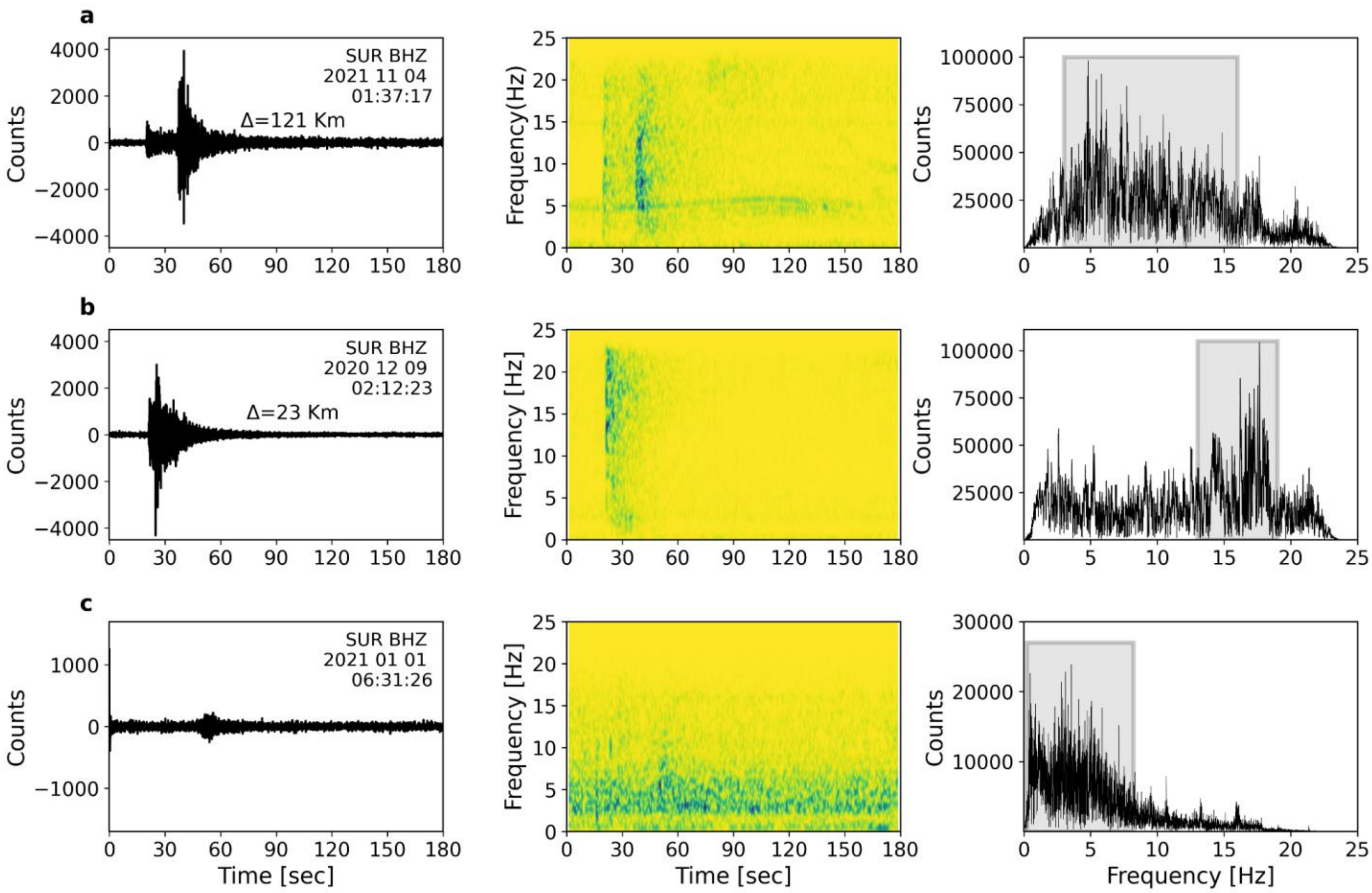

Figure 2: Examples of (A) an earthquake, (B) a blast, and (C) noise recorded at the SUR station. The station code, the component, epicentral distance (Δ) in kilometers, and the start time (UTC) of the chosen window are mentioned in the right corner of each waveform. The distinct spectral characteristics of each example can be seen in the corresponding frequency distribution (spectrogram) and frequency and amplitude distribution. Earthquake spectra exhibit two distinct frequency peaks corresponding to P- and S-phase arrivals, with predominant frequencies in the range of 3–16 Hz. Blast spectra show a single peak corresponding to the onset of the P-phase and have larger amplitudes in the higher frequencies between 12 and 18 Hz. Seismic noise amplitudes are generally lower and in the frequency range less than 5 Hz.

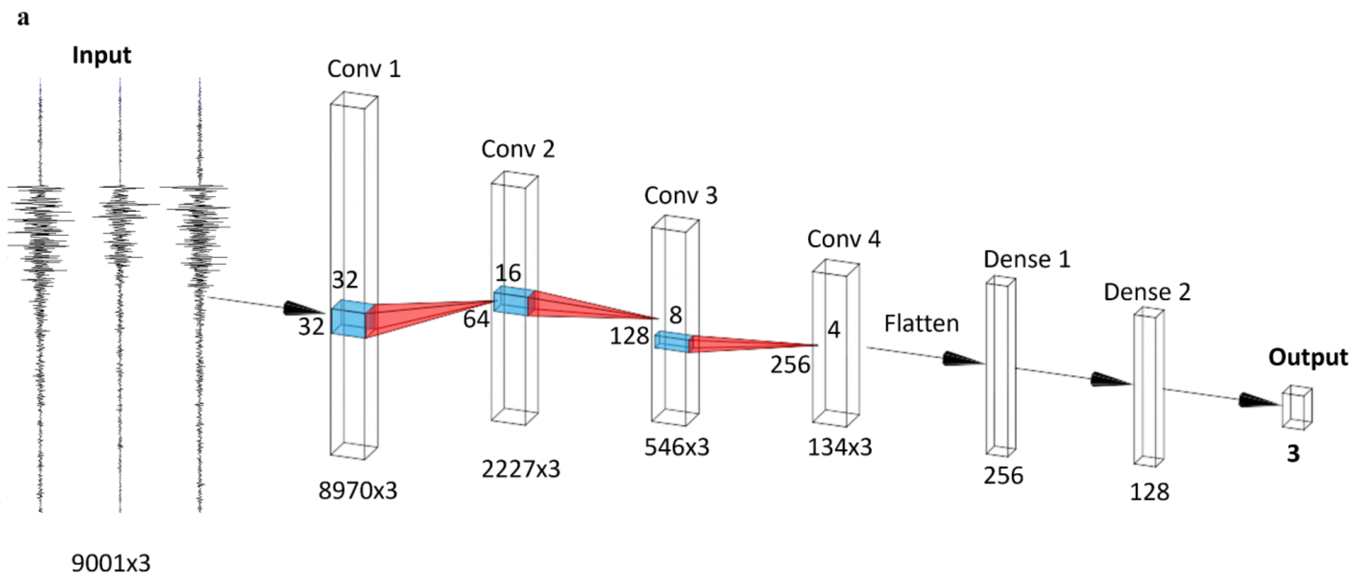

Figure 3(a): Schematic representation of the waveform-based CNN model's architecture developed in this study to discriminate between earthquakes, blasts, and seismic noise. The input for this model is a three-channel waveform of 180 seconds length at a sampling rate of 50 Hz. The input shape is (9001,3) corresponding to the number of points, and channels. This model was built with 4 1D CNN layers, with SeLU activation function. The output dimension is provided below each layer before the final prediction of the three classes (earthquakes, blasts, and seismic noise) using the softmax activation function.

b

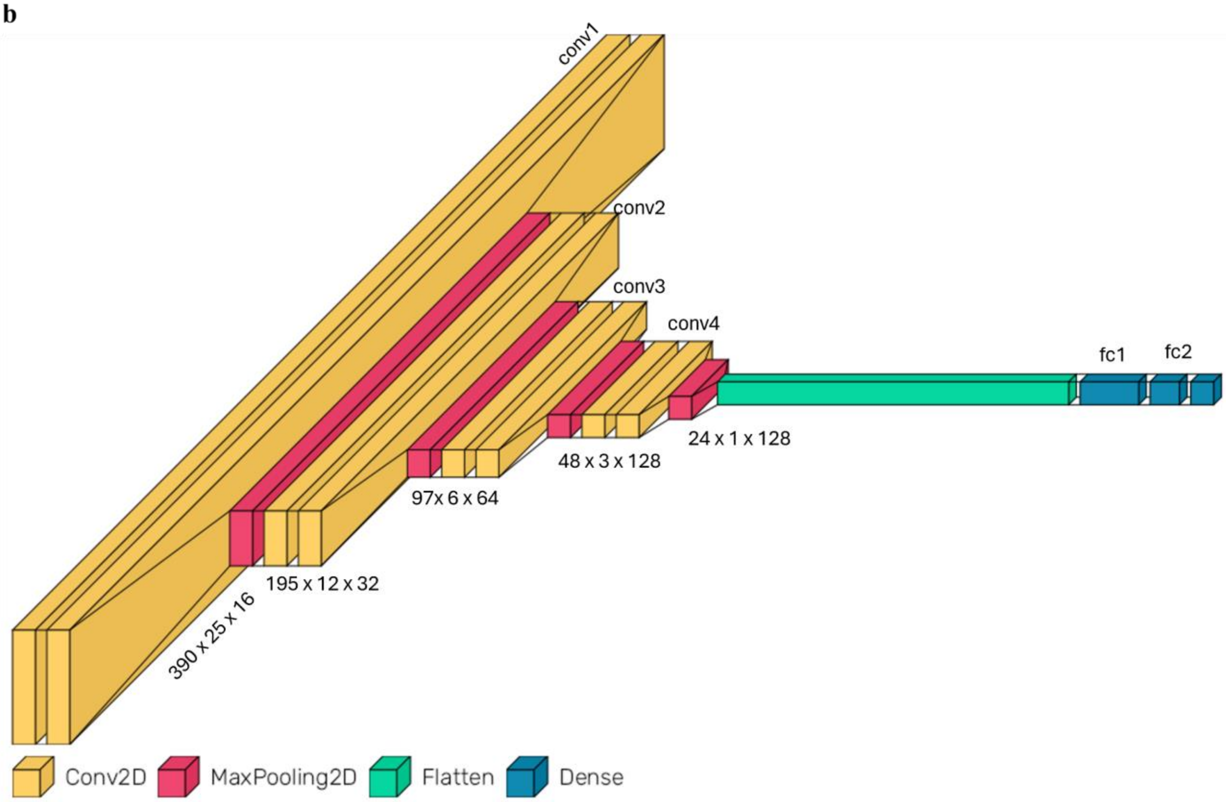

Figure 3(b): Schematic representation of the spectrum-based CNN model's architecture developed in this study to discriminate between earthquakes, blasts, and seismic noise. The input for this model is a three-channel spectrogram of 180 seconds length at a sampling rate of 50 Hz. The input shape is (390,25,3) corresponding to the number of points, frequency, and channels. The yellow block represents the 2D CNN layers which uses SeLU activation function followed by 2D MaxPooling layers (red blocks) which reduces the dimension of the input data from 390 to 24 before flattening the data for fully connected layers that will be used for the final prediction of the three classes of earthquakes, blasts, and seismic noise using the softmax activation function.

Application of Deep Learning to Seismic Event Classification in the Gujarat Region, India

D. Pragnath [1,3], G. Srijayanthi [1, *], Johannes Faber[2,4], Jonas Köhler[2,4], Wei Li[2],

Nishtha Srivatsava [2,4], Santosh Kumar [1], Sumer Chopra [1]

The supplementary information file contains 2 tables and 9 figures.

Table S1: Accuracy and loss function with varying batch sizes of waveform model. The bold text indicates the best accuracy.

Learning rate	***Batch size***	***Accuracy***	***loss***	***Early stop epochs***
10^{-4}	4	95.61	0.1123	73
10^{-4}	8	95.52	0.1193	122
10^{-4}	16	94.90	0.1425	64
10^{-4}	32	94.64	0.1456	68
10^{-4}	64	94.60	0.1584	100
10^{-4}	128	94.20	0.1711	73
10^{-4}	256	93.50	0.1962	94
2×10^{-4}	4	90.51	0.2980	70

2×10^{-4}	8	92.69	0.1829	71
2×10^{-4}	**16**	**95.32**	**0.1274**	**64**
2×10^{-4}	32	93.57	0.1798	36
2×10^{-4}	64	95.03	0.1304	100
2×10^{-4}	128	94.22	0.1621	52
2×10^{-4}	256	94.26	0.1682	65

Table S2: The Area Under the Curve (AUC) obtained for waveform (WF), spectrum (SPEC) and combined (COM) models for individual classes.

AUC	**Waveform**	**Spectrum**	**Combined**
Overall	0.98	0.93	0.98
Blast	0.98	0.92	0.98
Earthquake	0.97	0.90	0.97
Noise	0.99	0.96	0.99

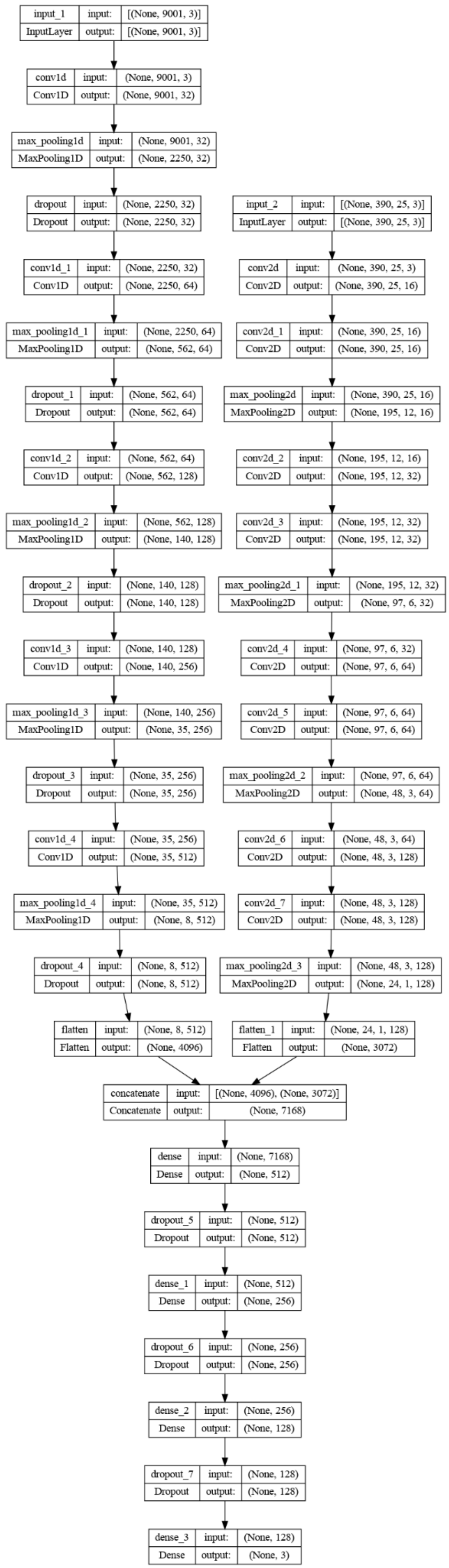
input_1 | input: | [(None, 9001, 3)]
InputLayer | output: | [(None, 9001, 3)]
conv1d | input: | (None, 9001, 3)
Conv1D | output: | (None, 9001, 32)
max_pooling1d | input: | (None, 9001, 32)
MaxPooling1D | output: | (None, 2250, 32)
dropout | input: | (None, 2250, 32)
Dropout | output: | (None, 2250, 32)
conv1d_1 | input: | (None, 2250, 32)
Conv1D | output: | (None, 2250, 64)
max_pooling1d_1 | input: | (None, 2250, 64)
MaxPooling1D | output: | (None, 562, 64)
dropout_1 | input: | (None, 562, 64)
Dropout | output: | (None, 562, 64)
conv1d_2 | input: | (None, 562, 64)
Conv1D | output: | (None, 562, 128)
max_pooling1d_2 | input: | (None, 562, 128)
MaxPooling1D | output: | (None, 140, 128)
dropout_2 | input: | (None, 140, 128)
Dropout | output: | (None, 140, 128)
conv1d_3 | input: | (None, 140, 128)
Conv1D | output: | (None, 140, 256)
max_pooling1d_3 | input: | (None, 140, 256)
MaxPooling1D | output: | (None, 35, 256)
dropout_3 | input: | (None, 35, 256)
Dropout | output: | (None, 35, 256)
conv1d_4 | input: | (None, 35, 256)
Conv1D | output: | (None, 35, 512)
max_pooling1d_4 | input: | (None, 35, 512)
MaxPooling1D | output: | (None, 8, 512)
dropout_4 | input: | (None, 8, 512)
Dropout | output: | (None, 8, 512)
flatten | input: | (None, 8, 512)
Flatten | output: | (None, 4096)
input_2 | input: | [(None, 390, 25, 3)]
InputLayer | output: | [(None, 390, 25, 3)]
conv2d | input: | (None, 390, 25, 3)
Conv2D | output: | (None, 390, 25, 16)
conv2d_1 | input: | (None, 390, 25, 16)
Conv2D | output: | (None, 390, 25, 16)
max_pooling2d | input: | (None, 390, 25, 16)
MaxPooling2D | output: | (None, 195, 12, 16)
conv2d_2 | input: | (None, 195, 12, 16)
Conv2D | output: | (None, 195, 12, 32)
conv2d_3 | input: | (None, 195, 12, 32)
Conv2D | output: | (None, 195, 12, 32)
max_pooling2d_1 | input: | (None, 195, 12, 32)
MaxPooling2D | output: | (None, 97, 6, 32)
conv2d_4 | input: | (None, 97, 6, 32)
Conv2D | output: | (None, 97, 6, 64)
conv2d_5 | input: | (None, 97, 6, 64)
Conv2D | output: | (None, 97, 6, 64)
max_pooling2d_2 | input: | (None, 97, 6, 64)
MaxPooling2D | output: | (None, 48, 3, 64)
conv2d_6 | input: | (None, 48, 3, 64)
Conv2D | output: | (None, 48, 3, 128)
conv2d_7 | input: | (None, 48, 3, 128)
Conv2D | output: | (None, 48, 3, 128)
max_pooling2d_3 | input: | (None, 48, 3, 128)
MaxPooling2D | output: | (None, 24, 1, 128)
flatten_1 | input: | (None, 24, 1, 128)
Flatten | output: | (None, 3072)
concatenate | input: | [(None, 4096), (None, 3072)]
Concatenate | output: | (None, 7168)
dense | input: | (None, 7168)
Dense | output: | (None, 512)
dropout_5 | input: | (None, 512)
Dropout | output: | (None, 512)
dense_1 | input: | (None, 512)
Dense | output: | (None, 256)
dropout_6 | input: | (None, 256)
Dropout | output: | (None, 256)
dense_2 | input: | (None, 256)
Dense | output: | (None, 128)
dropout_7 | input: | (None, 128)
Dropout | output: | (None, 128)
dense_3 | input: | (None, 128)
Dense | output: | (None, 3)

Figure S1: combined model architecture.

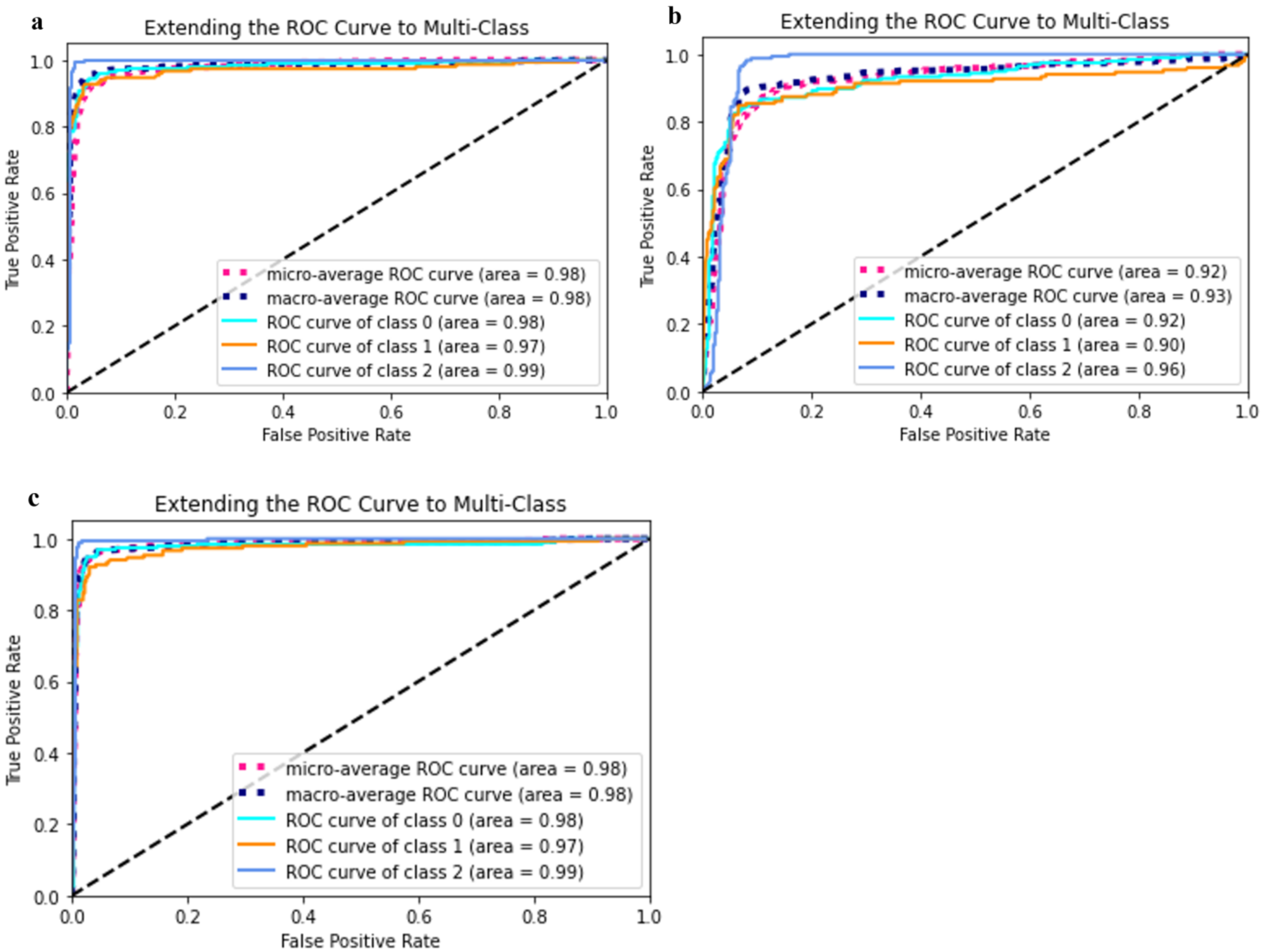

Figure S2: ROC plots of (A) Waveform model, (B) Spectrogram model and (C) Combined model.

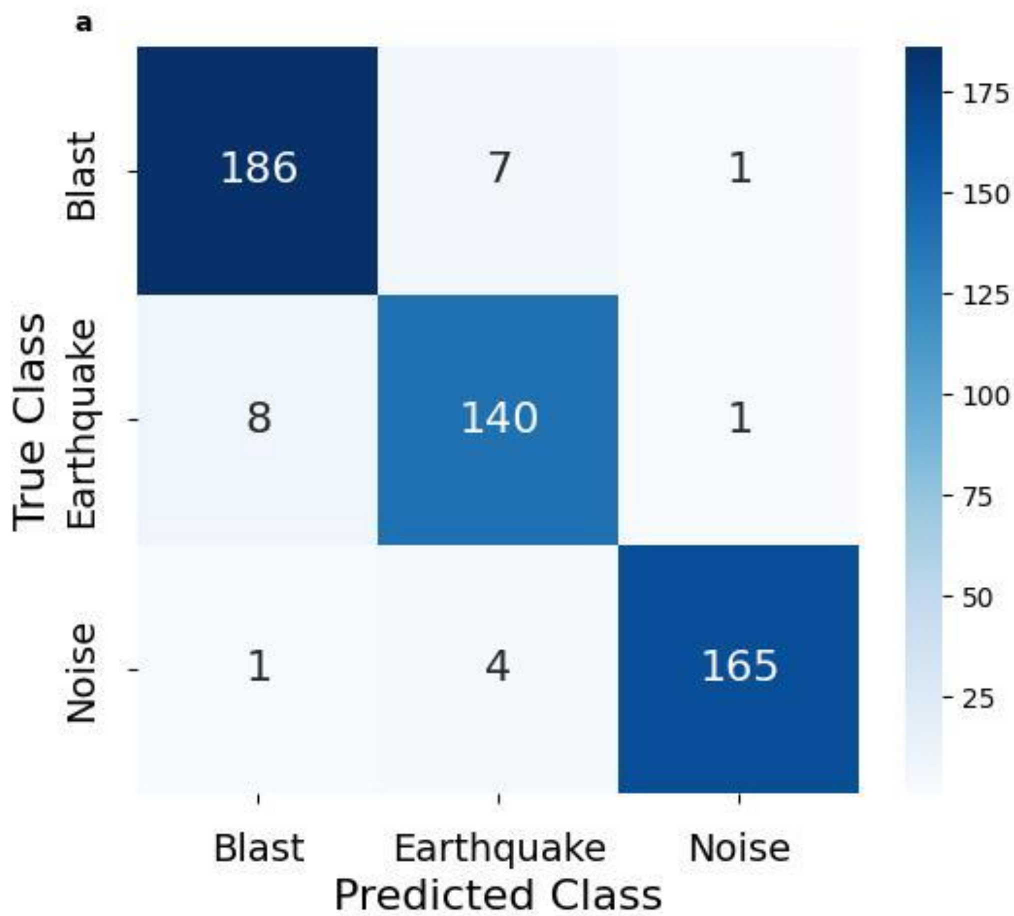
a
Blast
Earthquake
Noise
True Class
186
7
1
8
140
1
1
4
165
Blast
Earthquake
Noise
Predicted Class
175
150
125
100
75
50
25

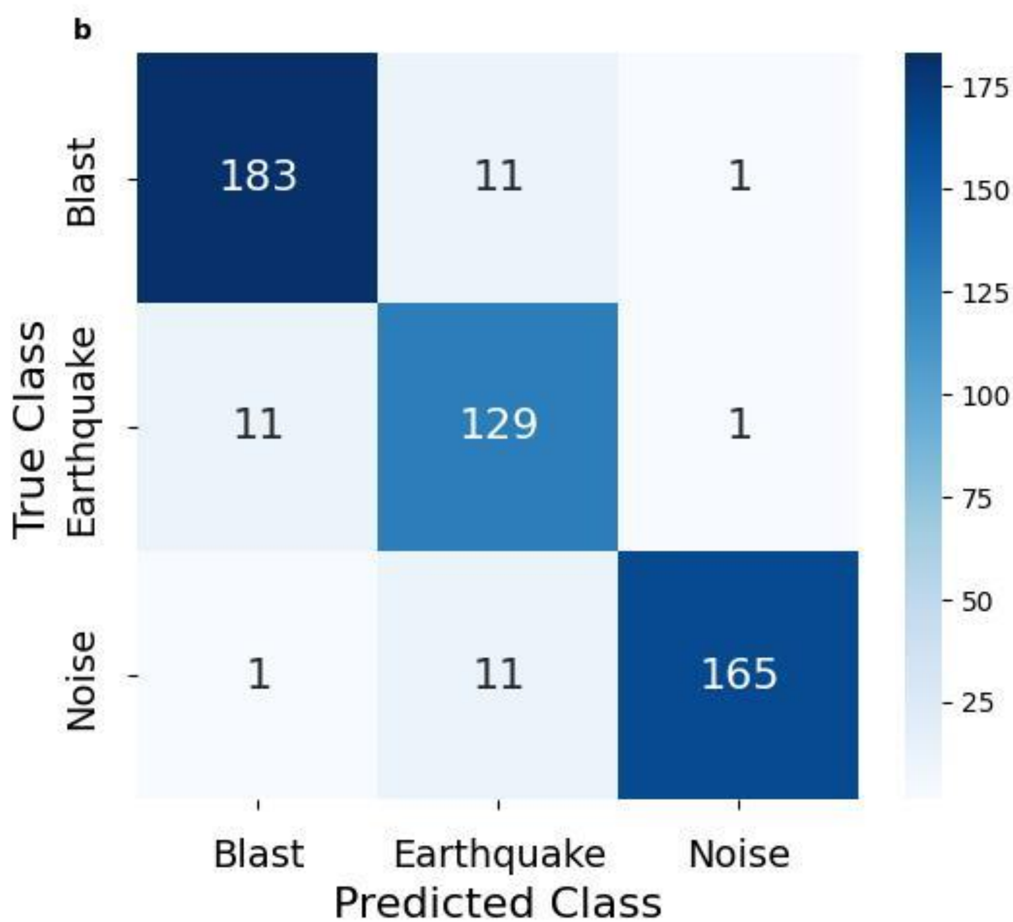
b
Blast
Earthquake
Noise
True Class
183
11
1
11
129
1
1
11
165
Blast
Earthquake
Noise
Predicted Class
175
150
125
100
75
50
25

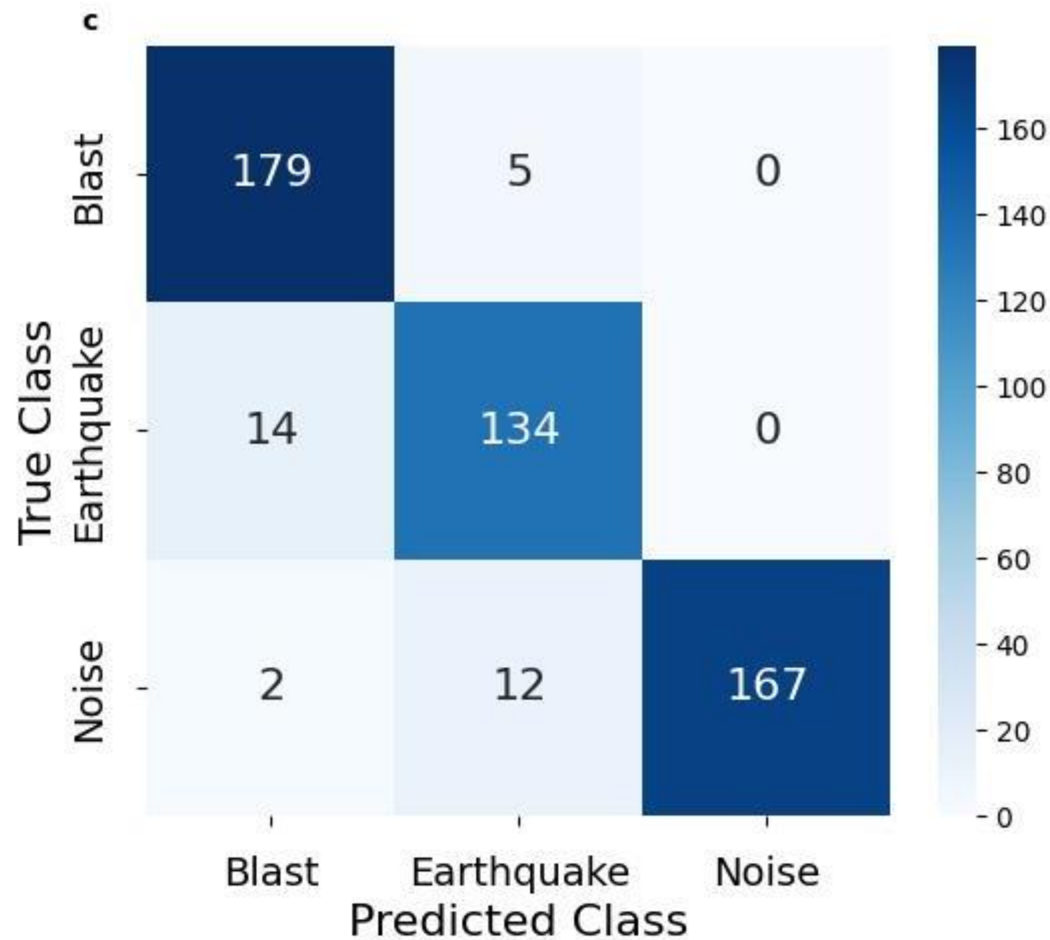

Fig. S3: Confusion matrices for analyzing and comparing the classification results obtained from three distinct models: (A) Waveform Model, (B) Spectrum Model, and (C) Combined Model.

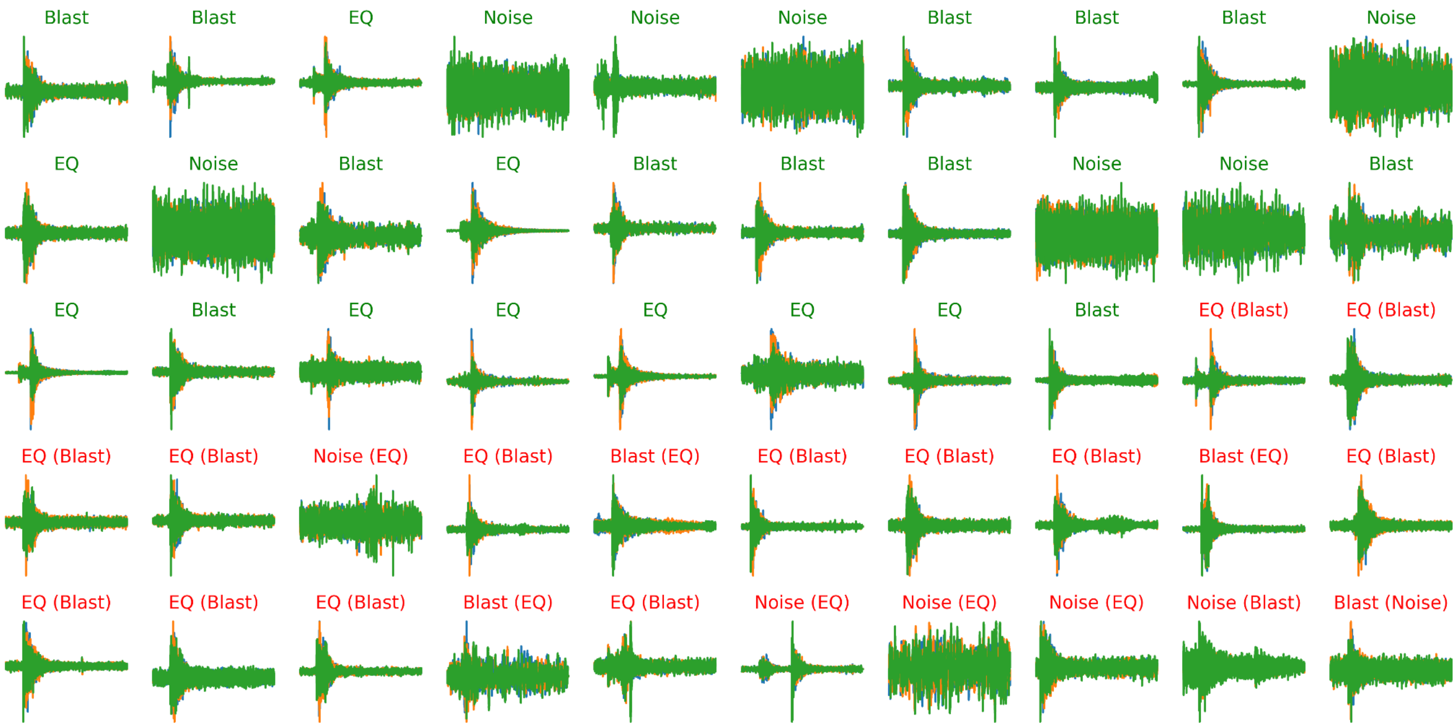

Figure S4: Visualization of test dataset traces along with their corresponding ground truth labels. The misclassified are shown in red colored font with the corresponding true labels in the brackets. It is evident that an increase in amplitude, especially when with poor signal-to-noise ratios led to classification errors.

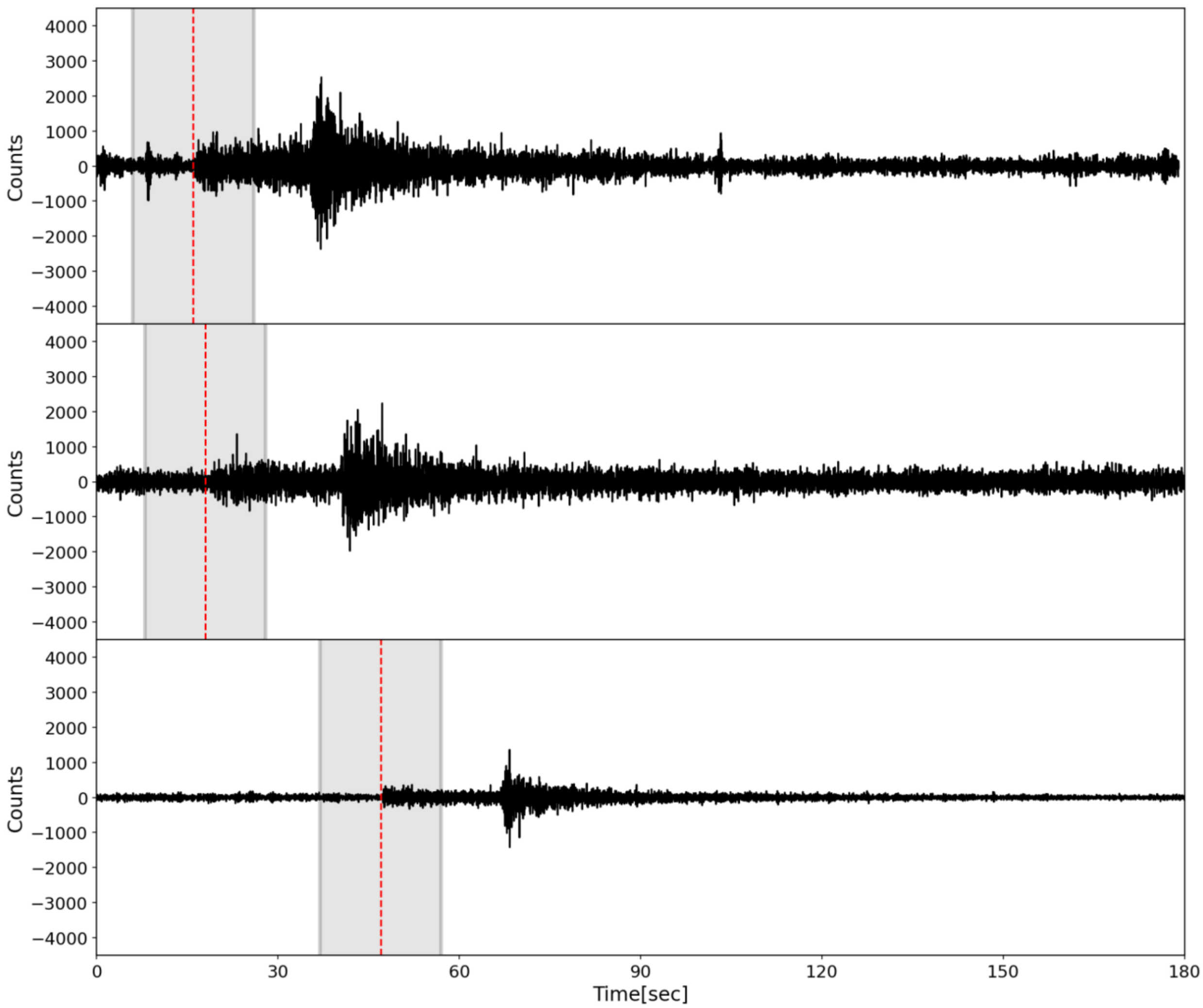

Figure S5: Examples of waveforms along with the selected window (gray shaded rectangle) to calculate the SNR. The dotted red line indicates the P phase, the shaded portion is a 20 s window, 10 s before and after P arrival each.

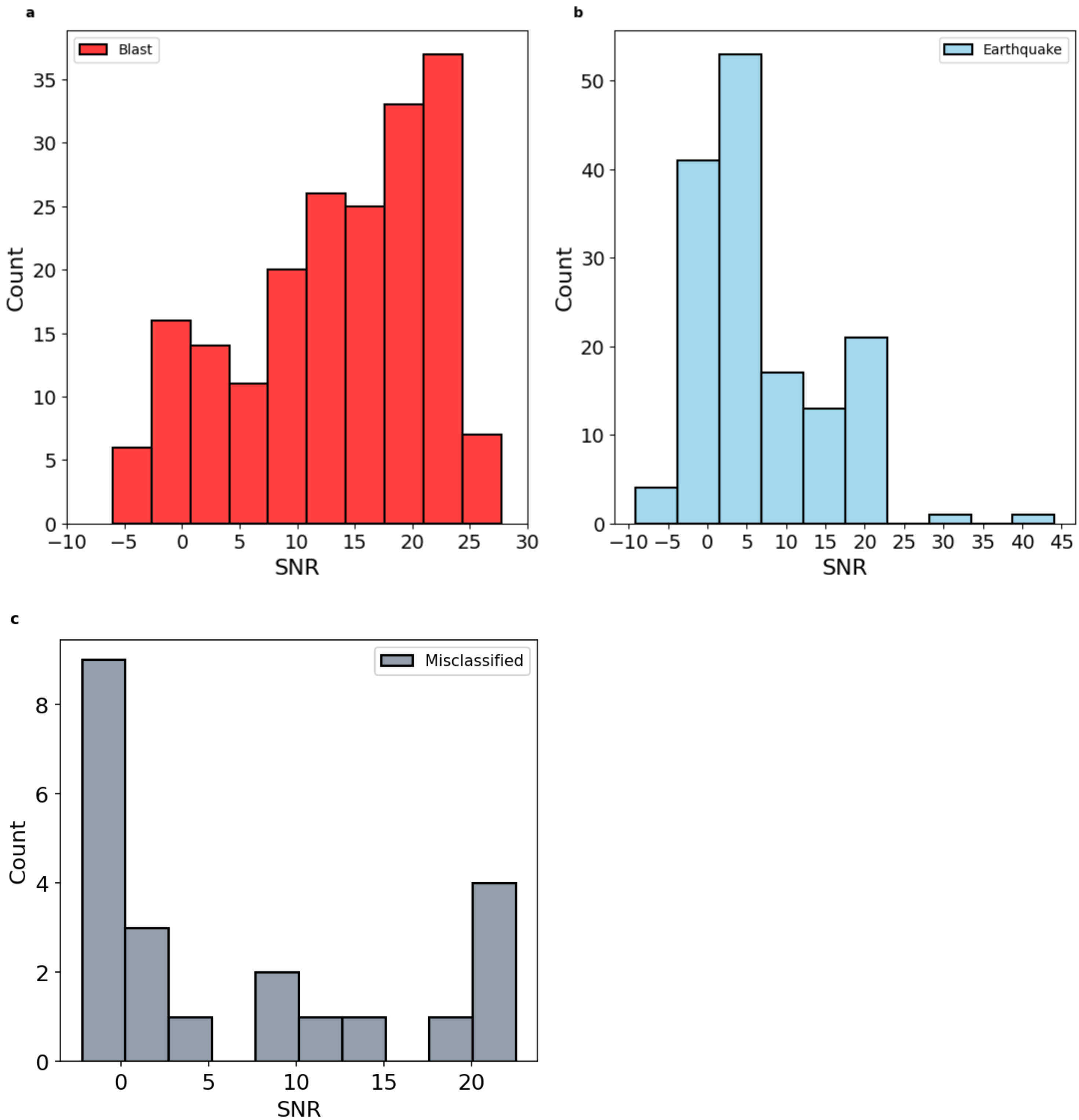

Figure S6: Signal-to-Noise Ratio of (a), (b), and (c) represents the SNR of blasts, earthquakes, and misclassified events, respectively, in the test dataset of the waveform model. When the strength of noise dominates over the signal, i.e., $\left(\frac{\mu\, S^2}{\mu\, N^2}\right) < 1$, negative values are observed. The SNR of all the waveforms (earthquakes (151) and blasts (195)) varies from -9 to 44 dB, indicating that noise dominates over the signal.

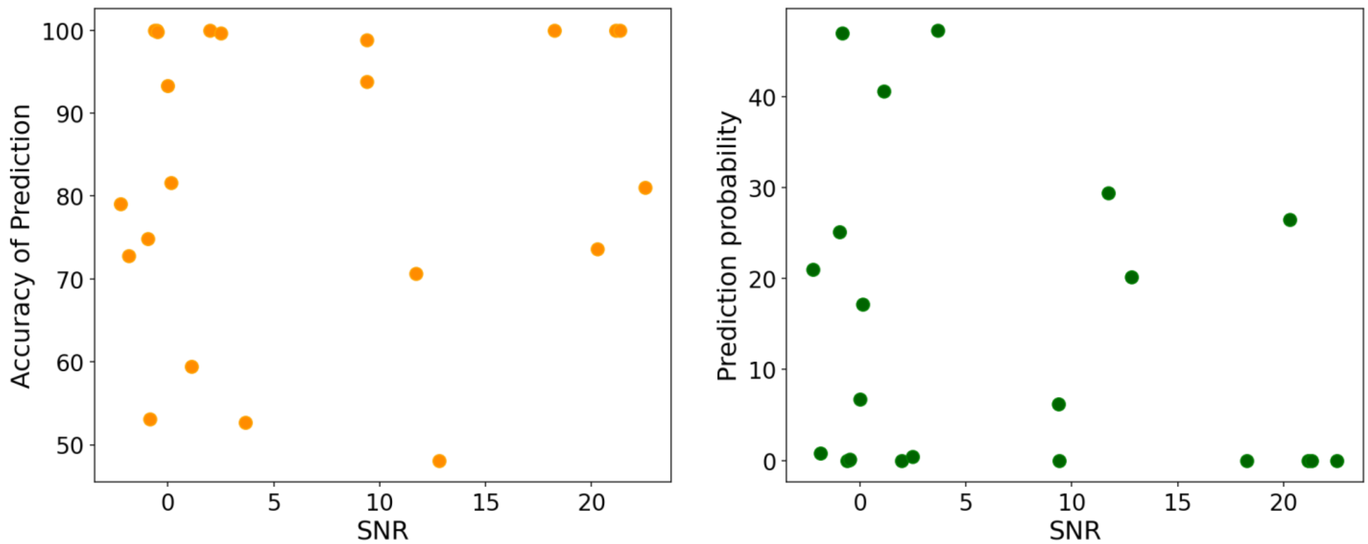

Figure S7: The figure shows the SNR values of the 22 misclassified events from the waveform model, along with the corresponding true (orange) and misclassified (green) prediction probabilities. The SNR is < 1 for 68% of the misclassified waveforms suggesting that the prediction probabilities for the true class are generally lower for misclassified waveforms with low SNR values.

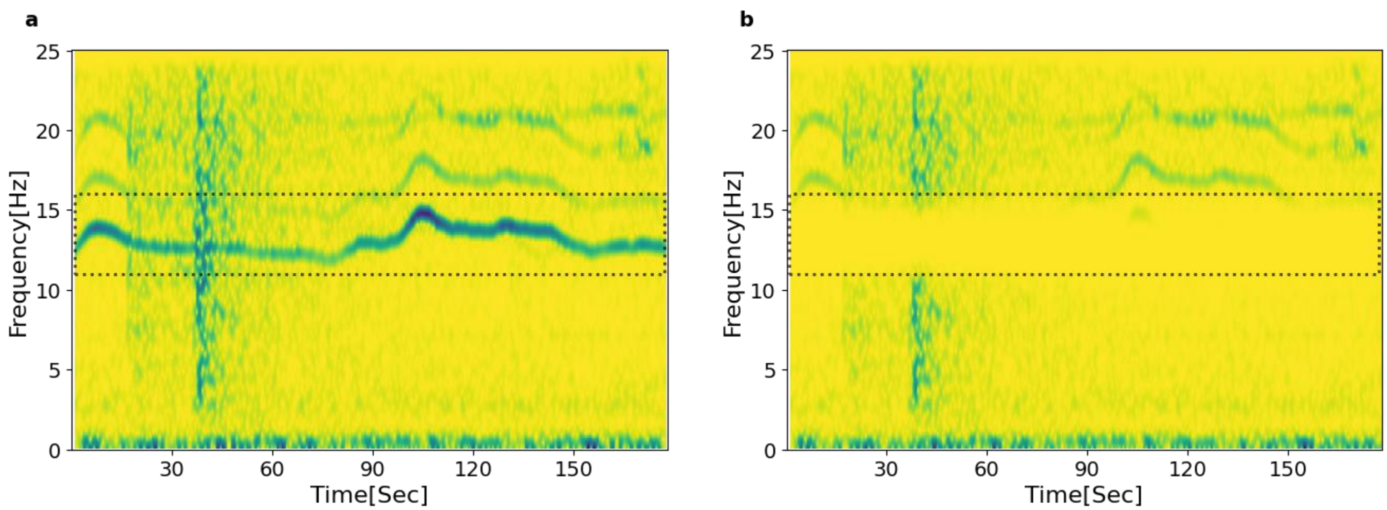

Figure S8: (a)Example of a misclassified spectrogram recorded at SUR station (on 2009-06-06 @ 10:27:42 GMT) showing three distinct energy bands within a frequency range through the selected time window. (b) Demonstrates the effect of applying a bandstop filter to attenuate these noise bands resulting in loss of information and a void at the filtered frequency band.

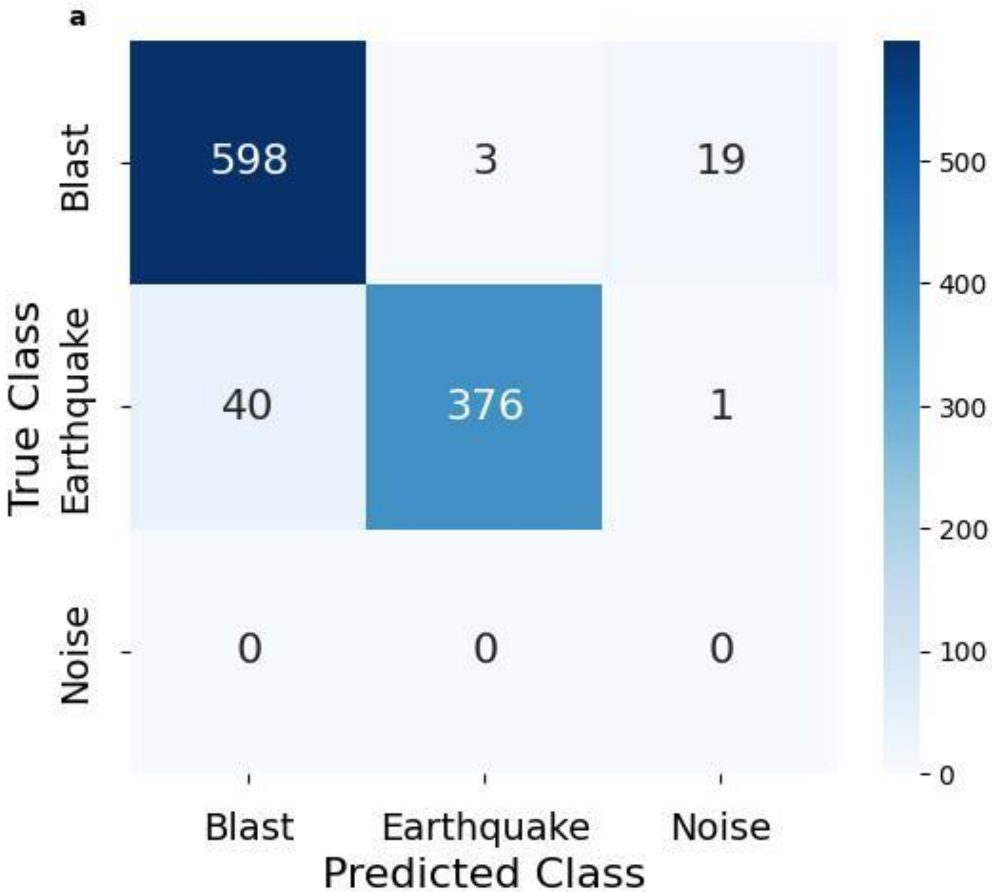
a
True Class
Blast
Earthquake
Noise
598
3
19
40
376
1
0
0
0
Blast
Earthquake
Noise
Predicted Class
500
400
300
200
100
0

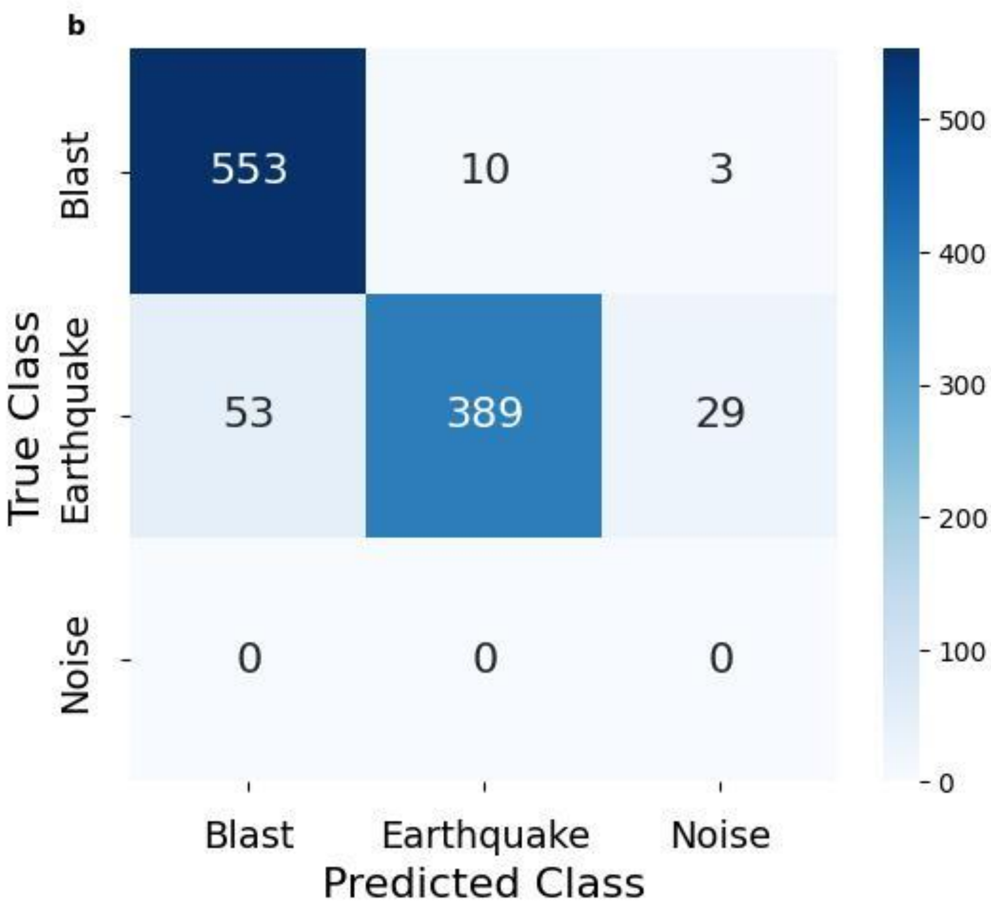
b
True Class
Blast
Earthquake
Noise
553
10
3
53
389
29
0
0
0
Blast
Earthquake
Noise
Predicted Class
500
400
300
200
100
0

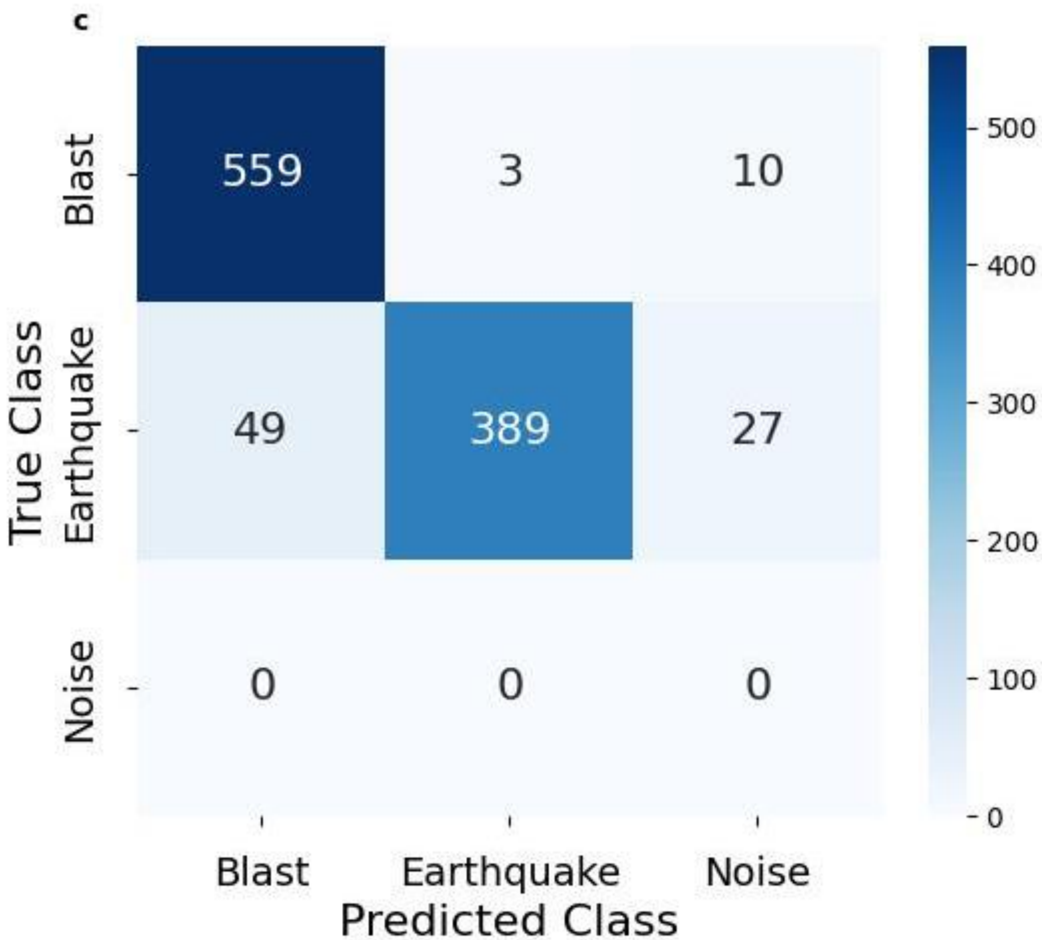

Fig S9: Confusion matrices for analyzing and comparing the classification results obtained from three distinct models: (a) Waveform Model, (b) Spectrum Model, and (c) Combined Model respectively when tested with data downloaded from SCEDC, on which the models are not trained.